tribology in industry

YU ISSN 0354-8996
VOLUME 19
SEPTEMBER 1997. 3

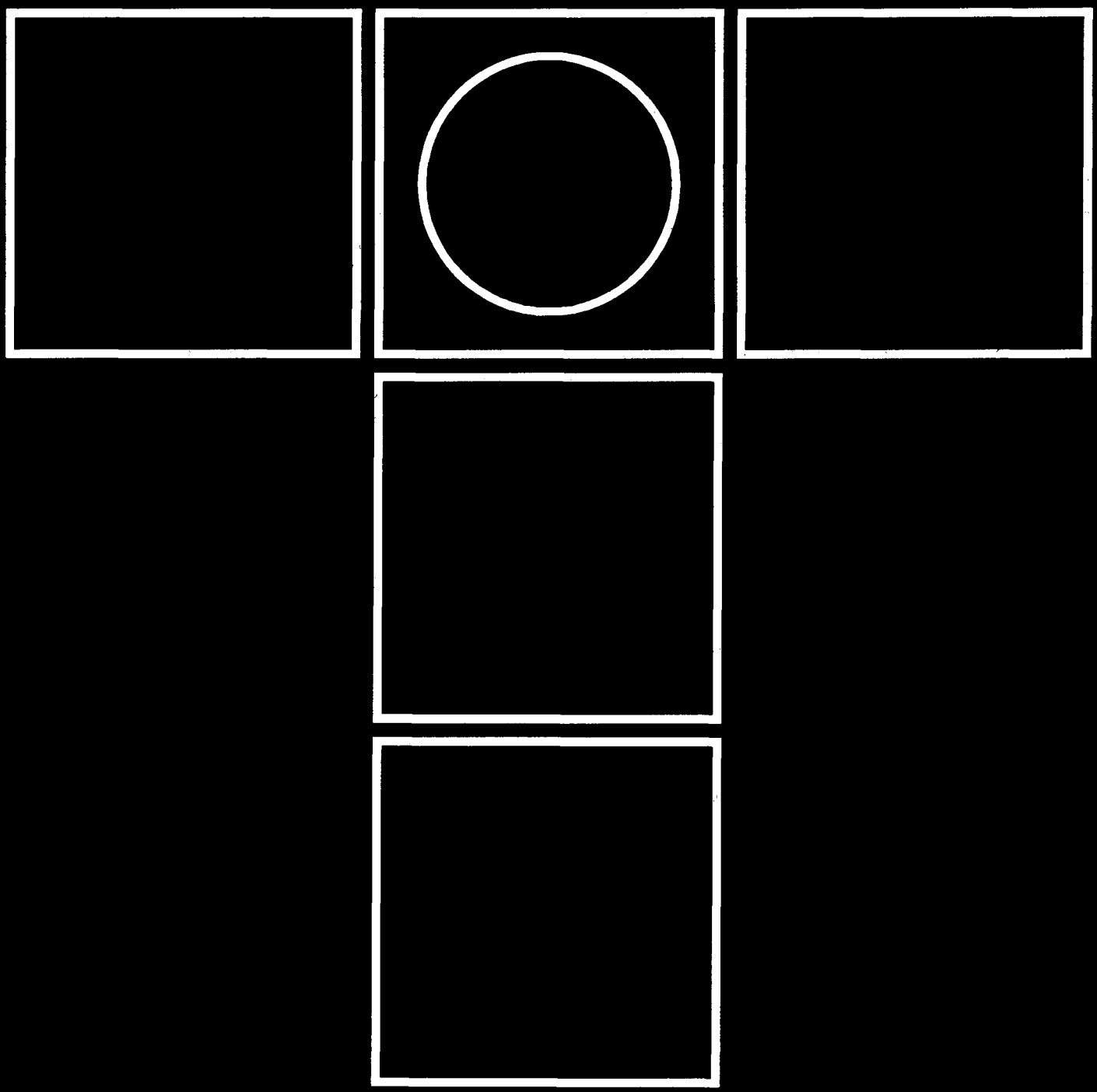

YU ISSN 0351 - 1642

VOLUME 19
Nº 3 (E)
SEPTEMBER 1997.

tribology in industry

contents

B. IVKOVIĆ

Tribological Approach to Manufacturing Costs in Industrial Systems

The quality of life and the living standard level of the population of any country depends, basically, on the labor productivity in all kinds of activities, and especially on productivity of industrial systems.

Industrial systems productivity is defined as the ratio of the realised added value in certain time interval (a month, a quarter, a year) and the spent labor measured either by number of workers or by number of hours.

The added value represents the difference between the realized income and costs in industrial system in the considered time period.

The manufacturing costs in industrial system arise, to the largest extent, due to consumption of material of different kinds, energy, machines, tools and other equipment that is used for realization of the manufacturing process.

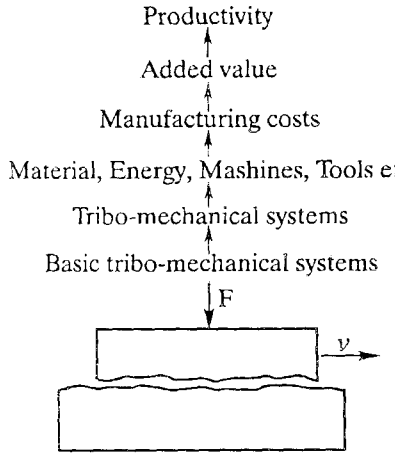

The value of total income, realized in the considered time period depends both on the quantity of products and on their price determined by the market.

The tribological approach to labor productivity increase of industrial systems is based on increase of the added value through decrease of the manufacturing costs.

The manufacturing costs are, basically, the consequence of tribological processes that are present in the contact zones of numerous tribo-mechanical systems that are part of manufacturing and other equipment during realization of the manufacturing processes.

The added value and productivity of industrial systems depend on intensity of tribological processes development in the contact zones of solid elements of numerous tribo- mechanical systems with, s a rule, presence of lubricant as the third element.

Upon the magnitude of the friction force in the contact zones of the basic tribo-mechanical systems is dependent the energy consumption in the manufacturing processes.

The second tribological process, the process of wear, leads to the appearance of the critical wear of one of the tribo- mechanical systems elements, and to the interruption of the production equipment work in order for the worn element to be replaced by the new or the regenerated one. The stops of the production equipment for the replacement of the worn element by the new one, as well as the cost of replacement, are increasing the manufacturing costs as a whole, and are decreasing the added value, namely the productivity of the industrial cistern.

The number of the basic tribo-mechanical in an industrial system of the medium size (circa 500 workers) in the metal working industry, depends on the type of the manufacturing equipment and it is around 400 000. The appearance of the critical wear of one of the elements of the tribo-mechanical systems always stops one part of the production process, and sometimes the process as a whole. Investigations show that the largest part of savings is being realised by application of the tribological knowledge to slowing down the wear process by use of the new tribomaterials, lubricants with the anti- wear additives, and, today already numerous, procedures for increasing the wear resistance of the contact layers of the solid elements of the tribo-mechanical systems.

The tribological approach to manufacturing costs in industrial systems is generally reduced to:

- knowing the tribological characteristics of material of the critical

tribo-mechanical systems elements,

- application of the modern lubricants with the anti-wear and anti-friction additives,
- introducing the tribomaterials and tribological coatings in manufacturing the elements of the tribo-mechanical systems,
- knowing the influence of the sliding speed and contact zone normal loading on the development of the wear and friction processes,
- application of the modern methods for increase of the wear resistance of the contact layers of the tribo-mechanical elements.

The tribological approach to the manufacturing costs is independent of the typean complexity of the manufacturing processes and equipment, since it is reduced to friction and wear problems in the contact zones of the basic tribo- mechanical systems.

UDK 621.9.025.004.6:621.941

K. -D. BOUZAKIS, K. EFSTATHIOU, N. VIDAKIS

The Failure Mechanism of PVD Coated Hardmetal Inserts in Milling

RESEARCH

The performance of PVD coated hardmetal inserts is significantly influenced by the mechanical properties of the cemented carbides as well as by the fatigue behaviour of their coatings. During interrupted cutting processes, such as milling, the cutting tool is subjected to impacting cutting loads that usually initiate the fatigue fracture of the compound, decreasing herewith the insert performance. The coating fatigue lifetime is predictable with the aid of developed procedures, as well as is well known the static strength of hardmetals. In this paper, the fatigue behaviour of coated inserts is examined experimentally and analytically in milling. The failure is depicted through Scanning Electron Microscopy (SEM) and Energy Dispersive X-ray (EDX) microspectral investigations of the examined cutting edges. Furthermore, through a Finite Element Method (FEM) simulation of the contact between the tool and the workpiece, the distributions of critical stress components that are associated with cohesive coating fatigue failure mode are determined.

Keywords: Coated inserts, Fatigue behaviour, Failure mechanism.

1. INTRODUCTION

Coated cutting tools have to operate within safe stress limits considering the coating endurance, especially in cases of cutting processes with discontinuous material removal [1, 2]. On the other hand, the strength of the cemented carbide may become a dominant insert failure parameter. In the following paragraphs, an analytical-experimental method to determine coating fatigue properties will be introduced. Furthermore, a FEM simulating procedure to determine the tool stress distribution, occurring during milling, is described. With the aid of this procedure, the experimentally obtained results in milling can be evaluated and the performance of cemented carbide substrates and of their PVD coatings can be predicted.

2. THE FATIGUE PERFORMANCE OF PVD COATINGS

The precise knowledge of the fatigue behaviour for various coating substrate compounds is of major importance for coated elements that are exposed to alternating operational loads. Coated tools in cutting processes with discontinuous material removal are typical examples. On that account, several tests that mainly describe the fatigue attitude of coatings qualitatively are being carried out, in order to find out the most promising combination of coating and base materials.

The impact test offers reliable quantitative information concerning the endurance limits of various coatings [3, 4, 5, 6, 7]. The test arrangement and typical experimental results for example for TiN coating are illustrated in figure 1. During the test, a plane coating substrate compound is exposed to an alternating Hertzian contact pressure, by impacting its surface through a cemented carbide ball, as it is shown in the upper left part of the figure. This test is capable to apply changeable impact force as well as frequency. Herewith, graphs of the impact load versus the number of successive impacts can be plotted as shown in figure. The dominant failure mode of this coating, according to Scan Electron Microscope (SEM) observations and Energy Dispersive X-ray (EDX) microspectrals, is cohesive and not adhesive, i.e. chipping and not delamination. In terms of critical stress components, a cohesive failure is designated by high principal stresses within the coating, in contrast to the adhesive failure mode, where the hazardous potential stress component is high shear stress along the coating substrate interface [7, 8].

The FEM simulation of the impact test, in association to the entire examination of the tested specimens, can provide values for critical mechanical stress components, that caused the cohesive surface fracture of the coating. In order to accelerate the test, heavy loads are being applied and the consequence is the plastic deformation of the substrate material. Therefore, during the impact

Prof. Dr. -Ing. habil K. -D. Bouzakis,
Lecturer Dr. -Ing. K. Efstathiou,
Research Fellow Dr.-Ing. N. Vidakis
Laboratory for Machine Tools and Machine Dynamics,
Aristoteles University Thessaloniki, Greece

test, the elastic coating is loaded within a stress alteration that has a non-zero minimum value, due to the substrate plastic strain. Basic material properties, that are essential for the FEM simulation, such as elasticity moduli and stress limits, are obtained through nanohardness tests for the coatings as well as for the substrate materials [9]. The stress limit for hard cutting tool TiN coating is assumed to be its yield stress, since it is brittle material.

Furthermore, the Smith diagram of TiN coating, that is widely used in cutting tool applications, is presented in the middle part of figure 1. During the cutting phase, the coating deforms purely elastically, and due to the lack of plastic deformation within the cutting edge recovers completely to the initial position by the end of the contact with the workpiece. On that account, the stress limit for the coating is derived from the region A-B of the Smith diagram that has a zero minimum stress. This value and the static stress limit, i.e. the coating yield stress are used to compose the Woehler diagram as it is also presented in the lower part of figure 1. This diagram will be used subsequently to exhibit the effect of certain parameters on the coating fatigue behaviour.

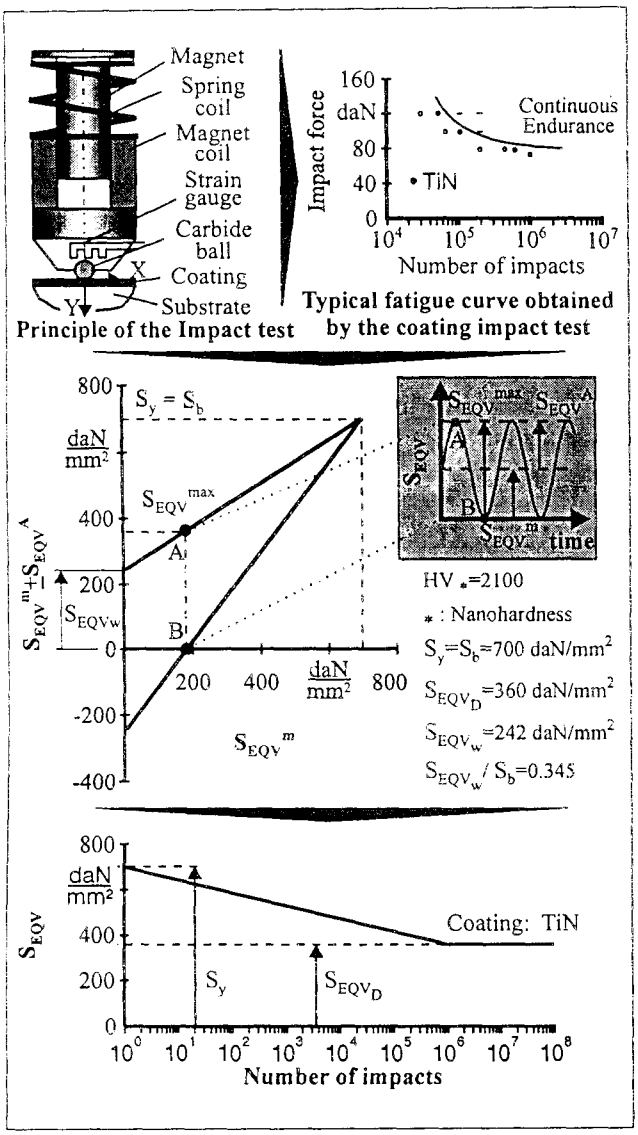

Fig. 1: Determination of the fatigue properties of thin hard coatings using the impact test and derived Smith and Woehler diagrams for the TiN coating.

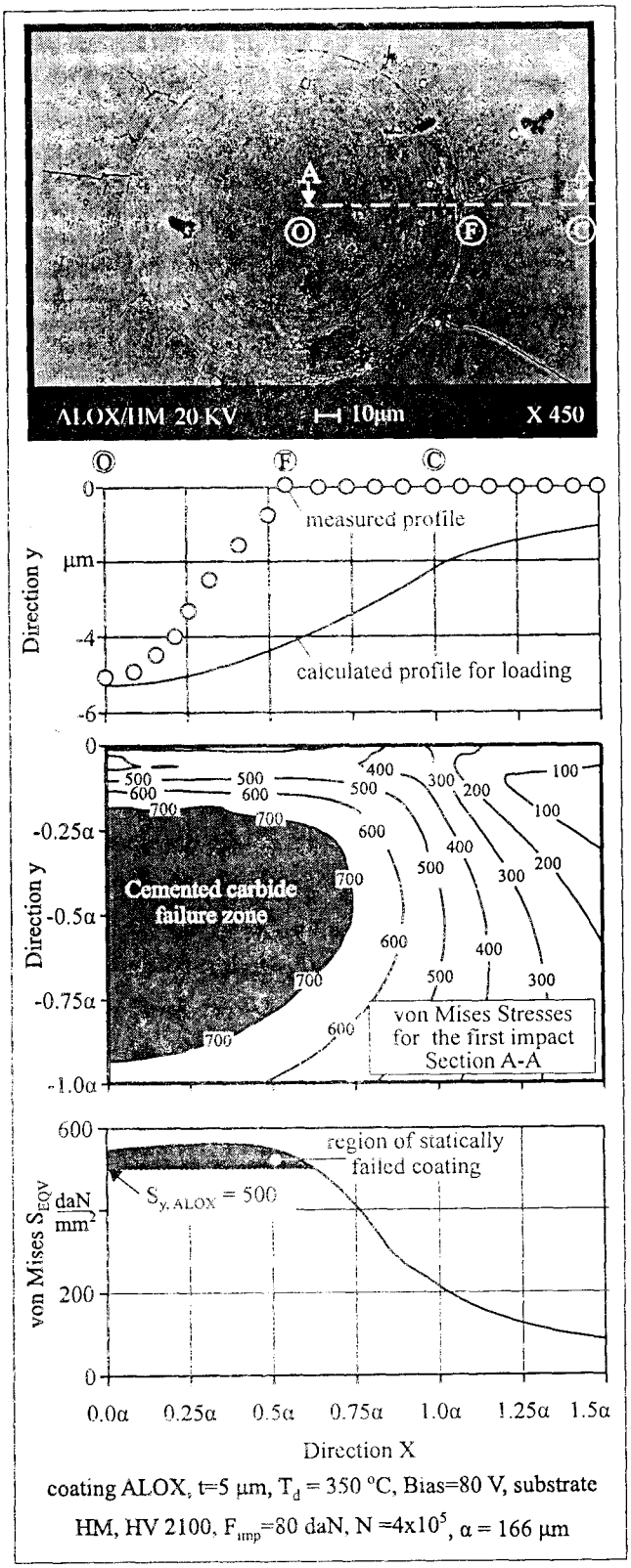

Fig. 2: Typical failure mode of cemented carbide substrate, coated with a multilayer coating, during the impact test, and FEM explanation.

3. THE BEHAVIOUR OF HARDMETALS IN IMPACTING LOADS

The application of the impact test on a graded A1203 and TiAlN multilayer coating, deposited on cemented carbide substrate, illustrated the behaviour and the performance of hardmetals in impacting loads, relative to the ones developed in milling [4]. As base material, ultra fine-grained cemented carbide was selected, having a hardness of *2100 HV*. Owing to this improved homogeneous structure, the static stress limit for the base brittle material was reasonably assumed to be the one third of its Vickers hardness, i.e. *700 daN/mm*^{2}.

The upper SEM photograph of figure 2 indicates a pure cohesive coating failure, declared by circumferential and radial microcracks. The further inserted measured imprint profile indicates a quite deep imprint. The substrate collapse between positions *O* and *F* covers only a portion of the developed contact circle. The intense applied impact load, in combination with the very high stiffness of the contact bodies, led to the development of extremely high contact pressures, taking into account the inability of the pairing materials to form an expanded contact circle, due to the lack of any hardening rule.

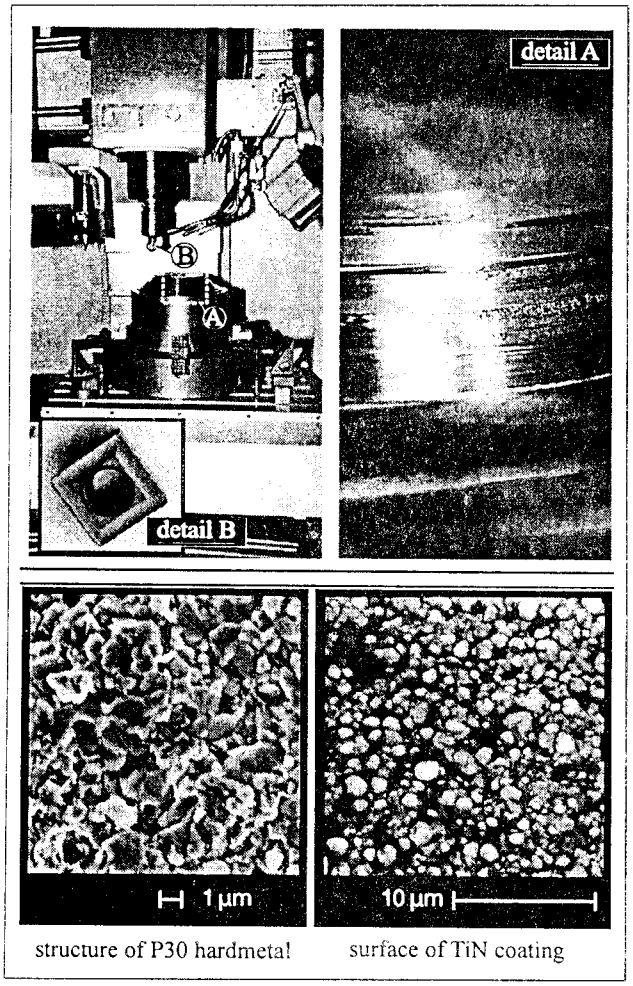

Fig.3: The experimental configuration, the produced workpiece surface and details of the coated insert

Based on these remarks, the developed FEM model, which simulates the impact test, was adjusted to this specific configuration. Since hardmetals are extremely brittle materials, the surmounting of their yield stress leads to intrinsic coherence release and subsequent fracture. This behaviour was attributed to the substrate by assuming an elastic perfectly plastic response, preventing herewith a non-reasonable hardening mechanism. Under these circumstances, the calculated loaded imprint profile is also penned besides the measured one.

The corresponding FEM stress results are presented by the stress distributions inserted in the bottom of figure 2. The region of the substrate material that exceeded its static stress limit is bounded in the shaded area of section *A-A*, which is in a very good agreement with the corresponding imprint profile, since they have identical coordinates. It must be mentioned that the von Mises stresses in the shaded area are produced by the three-axial compressive stresses that appear in this position during Hertzian contacts. That is the reason for the non-recovered profile between positions *O* and *F* after the end of each penetration. Furthermore, the observed coating cracks are in accordance to the superficial distribution of von Mises stresses that show the region of the coating surface that is out of its static stress limit.

4. MILLING EXPERIMENTAL PROCEDURE

During the milling experimental stage, coated cemented carbide inserts were investigated in cutting conditions with discontinuous material removal, using a four-axes machining center. In the upper part of figure 3 the used tool-workpiece system is presented. The necessary preestimated number of successive cuts was accomplished by following sequential cyclic paths prescribed by the corresponding NC code. On the other hand, detail A at the upper right part of the same figure illustrates the produced workpiece surface along the circumference of each tool trace. The optical observation of such produced surfaces, the level of machining noise as well as the color of the formed chip were also indications for the insert condition after each specific experiment. In every case dry cutting was performed and air jet was selected to be coolant and chip remover.

The two micrographs inserted in the bottom part of figure 3 illustrate respectively the structure of the P30 cemented carbide substrate and a superficial aspect of the used TiN coating. In the first case the micrograph refers to a brittle broken insert and illustrates the sintered carbide grains within a cobalt matrix. On the other hand, the surface of the coating exhibits a cionic development along the direction of its depth conducted du-

ring the sputtering process. Both micrographs refer to non-used cutting inserts and illustrate their initial status.

Each experiment was conducted by holding stable all cutting parameters and inspecting the coated edge after a predetermined number of successive cuts. The insert inspection after each distinct experiment was carried out by means of Scan Electron Microscopy and Spectroscopy as it is further described.

5. THE FEM SIMULATION OF THE MILLING PROCCESS

Due to the selected cutting edge geometry during milling, the cutting edge is stressed uniformly along a length corresponding to the axial cutting depth and to the positioning angle of the insert. For the cutting tool, this stress situation corresponds to a typical plane strain problem, supported by the majority of commercial multi-purposes FEM packages. In this way, the three- dimensional problem can be reasonably reduced to a two-dimensional one, permitting herewith the exploitation of the CPU resourses for the development of finer nodes net and decreasing the discretization error that the three dimensional simulation introduces.

The utilized modeling strategy is illustrated in figure 4. The tool-workpiece system is simulated by the plain strain nodel of the coated cutting edge. The acting cutting loads are applied in a form of superficial normal and tangential pressure distributions obtained using the entire cutting kinematics, the predetermined cutting forces and the chip compression ratio. Both coating and carbide substrate are assumed to be perfectly bonded together, whereas interfacial slip is not allowable. The simulation considers uniform coating thickness along the rake and the free faces respectively, and a film that follows the curvature of the carbide substrate at the tip of the cutting edge. To develop a reproducible FEM model capable of prescribing stress distributions, independent of geometric and dynamic restrictions the simulation was carried out parametrically, using a design language that the employed FEM package ANSYS.53 supports [10]. Thus, the coating thickness, the undeformed chip dimensions, the cutting forces and the model dimensions are variable and changeable parameters per machining case.

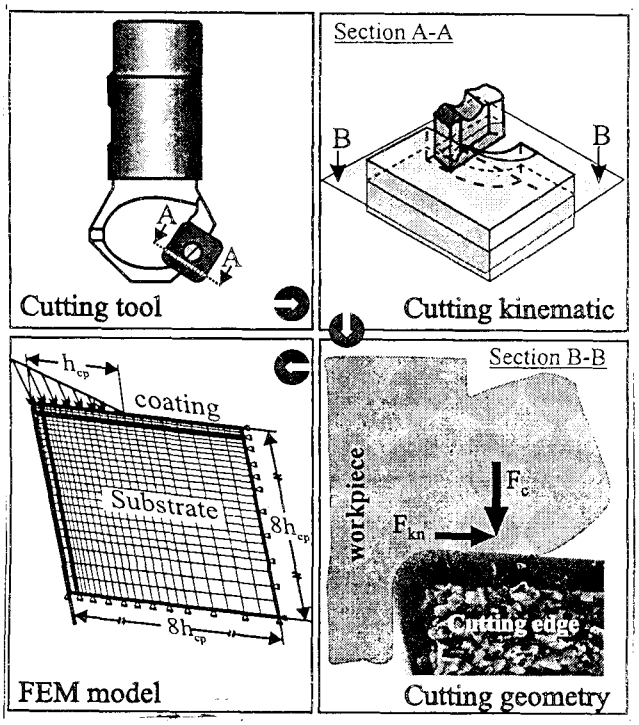

Fig. 4: The FEM simulation of the cutting proccess

The aforementioned FEM simulation of the milling process required material and technological data related to the cutting loads and the contact geometry. Taking into account that these magnitudes depend on the tool geometric configuration, the cutting kinematics and the workpiece material components, to proceed to a reliable simulation, such data were experimentally determined. The upper part of figure 5 illustrates the normal and tangential to the rake face force components versus the used feedrate, i.e., the dimensions of the undeformed chip thickness. The cutting forces were expressed according to the Kienzle-Victor equations:

$$F_c = K_c \cdot b \cdot h_{cu}^{1-mc}, \qquad F_{kn} = K_{kn} \cdot b \cdot h_{cu}^{1-mc}, \qquad (1,2)$$

as functions of the undeformed chip dimensions. The coefficients of these equations are also inserted in figure. Furthermore, the chip compressibility, being expressed by the chip compression ratio, was also experimentally determined for the used 42CrMo4 V workpiece material and is also penned in figure 3. It may be observed that the chip compression ratio decreases as the undeformed chip thickness rises [2]. On the other hand the use of coated inserts leads to the production of less deformed chip than the corresponding of conventional uncoated ones, due to the reduction of the acting friction obtained by the tribologically superior coating.

6. FEM SUPPORTED INTERPRETATION OF THE EARLY TIP BREAKAGE

During the entirety of the cutting experiments, the coated carbide inserts illustrated an unvaried attitude regarding their failure mechanism, constituted by early carbide failure at the tip of the cutting edge. This breakage of the cutting edge is illustrated in the three SEM micrographs of figure 6 for inserts used in three different feedrates. Consecutive solutions of the FEM model for successive positions of the cutting edge, within the workpiece material, enabled the stress interpretation of the

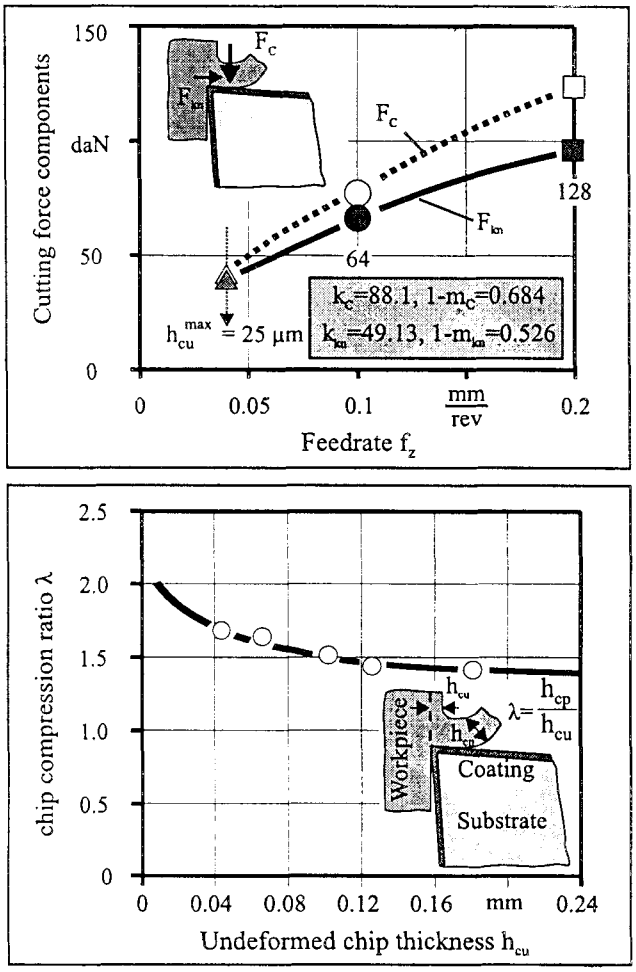

Fig.5: The cutting forces and the chip compressibility versus the dimensions of the undeformed chip γ =11.5", α=11", κ=45", b=5.67 mm, v=100 nt/min, tool P30, coating TiN, t=4 µm, workpiece 42CrMo4V, R_m=105 daN/mm^2

observed immature carbide failures. On the other hand these FEM solutions explained why the early tip breakage was independent from the activated feedrate.

Figure 7a illustrates the progress of the normal compressive or tensile stresses in successive positions of the tool during one penetration into the workpiece material. Since sintered carbide inserts are brittle materials, the maximum normal stress is more convenient to be used as failure criterion (Rankine criterion). In every position, high compressive stresses occur on the rake face, whereas high tensile stresses exhibit the free face near the tip of the cutting edge. A remarkable point is that the stress development does not exhibit a monotonous behaviour, illustrating a critical revolving position, where the aforementioned stresses take a maximum value, as shown in the right diagram of figure 7b. The left diagram of figure 7b states that in every utilized feedrate the undeformed chip thickness takes its critical value, regarding the resulting maximum normal stress, in different revolving positions within one penetration of the cutting edge. Taking into account the right diagram in figure 7b, where the stress components are inserted versus the undeformed chip thickness, the correlation between the presented stress distribution and the observed tip failure is evident.

The reason for this stress behaviour, that is significantly dependent on the cutting parameters and the workpiece material, can be explained considering the values of the cutting forces and the contact geometry. The developed contact pressure derives from the cutting forces normalized to the contact area. Both magnitudes are non-linear and experimentally determined functions of the undeformed chip dimensions. Herewith the contact pressure

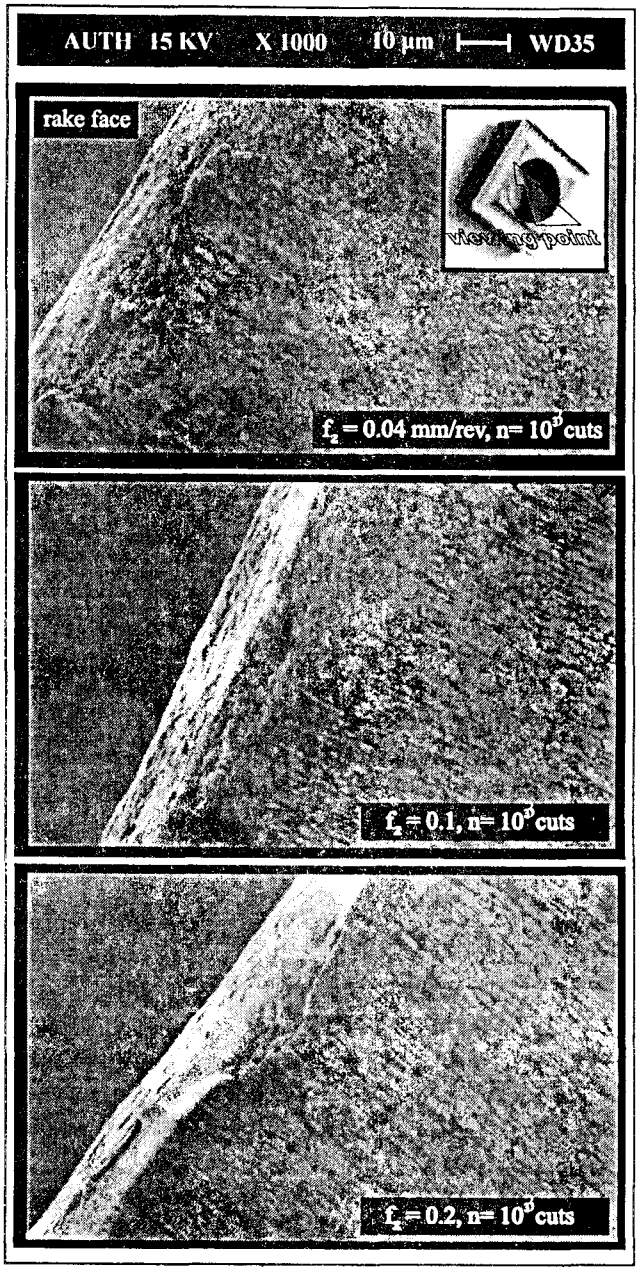

Fig. 6: Aspects of the tip breakage of the cutting edge for various feedrates γ = 11.5", α=11", κ=45", b=5.67 mm, v=100 m/min, tool P30, coating TiN, t=4 µm, workpiece 42CrMo4V, R_m=105 daN/mm^2

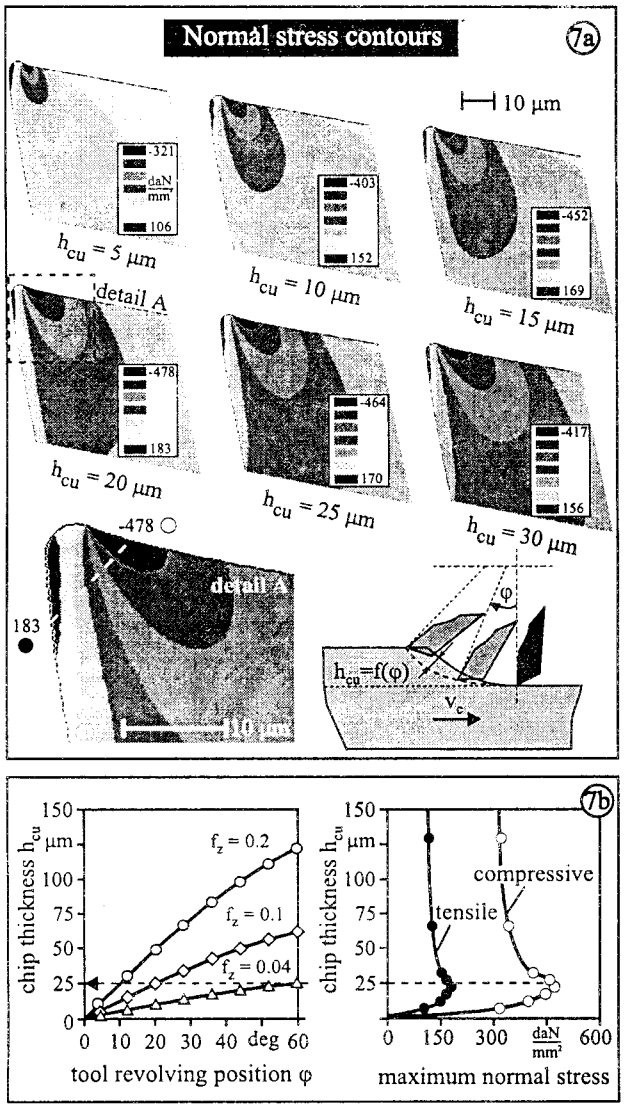

Fig. 7: The course of the developed compressive and tensile normal stresses and their dependency on the feedrate $\gamma = 11.5°$, $\alpha = 11°$, $\kappa = 45°$, $b = 5.67$ mm, $v = 100$ m/min, tool P30, coating TiN, $t = 4$ µm, workpiece 42CrMo4V, $R_m = 105$ daN/mm²

attitude is not supposed to follow a constant law, since it is the correlation of two non-linear magnitudes.

The upper part of figure 8 illustrates the static compression and tensile stress limits of hardmetals as a function of the cobalt content percentage [11]. In the present case, where the P30 hardmetal was selected as base material, its specific stress limits besides the maximum occurring stresses are presented in the lower part of the same figure. As it is apparent, the permitted stress limits are surmounted by the occurring stresses during cutting and therefore the tip of the cutting edge fails. Since in every selected feedrate the cutting edge encounters this critical position, it is reasonable why the cutting edge always was damaged. The solution for such a problem could be the use of different cutting edge geometry with higher radius on its tip.

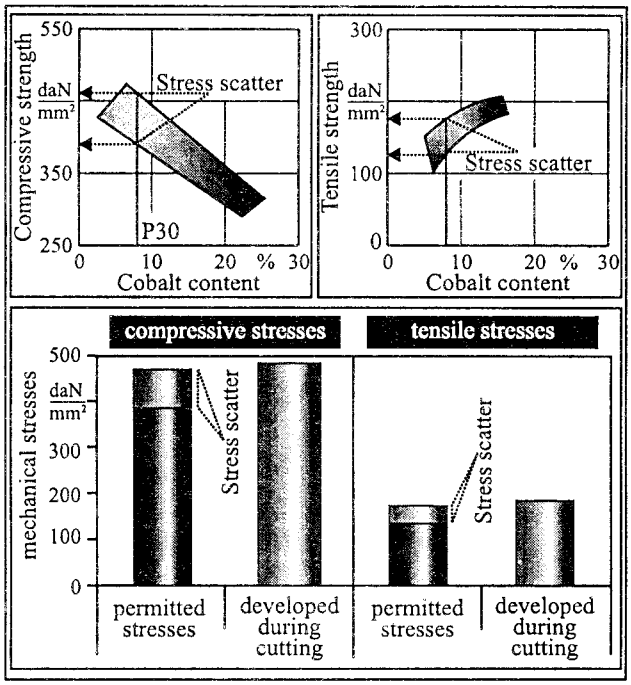

Fig. 8: Comparison between the developed normal stresses within the cutting edge with the corresponding permitted ones $\gamma = 1$ I.5", $\alpha = 11°$, $\kappa = 45°$, $b = 5.67$ mm, $v = 100$ m/min, tool P30, coating TiN, $t = 4$ µm, workpiece 42CrMo4V, $R_m = 105$ daN/mm²

The progress of the tip breakage of the cutting edge is illustrated in figure 9. In the first micrograph of part I of this figure, the plan view of such a failed cutting edge is presented at a low number of cuts. The whole aspect exhibits the tool rake face. The damaged tip is the light colored area on the left of the rake face. Moreover, the lower micrograph of the same figure part illustrates an oblique aspect of the same cutting edge. This view states that the tip damage forms a chamfer to the rake and the free faces of the cutting edge, replacing herewith the round fillet existing there before the fust cuts. The coating on the rake and the free faces respectively remains undamaged besides the broken tip, as it will be further described. Taking into account the dimensions of this chamfer projection on the rake face (*10-15 µm* approximately) in comparison to the whole tool- workpiece contact, the coating keeps operating sufficiently. This remark was validated by the high quality of the produced surface for as long as the remaining coating had been effective.

The observed tip damage of the cutting edge exhibited a standard progress as it is presented in part II of figure 9. The early-formed chamfer increases in length and reduces its angle with the rake face as the accumulated number of successive impacts rises. Both aspects of the cutting edge exhibit this behaviour. On the other hand it is obvious that in this high number of successive cuts the coating had started loosing its intrinsic coherence, orien-

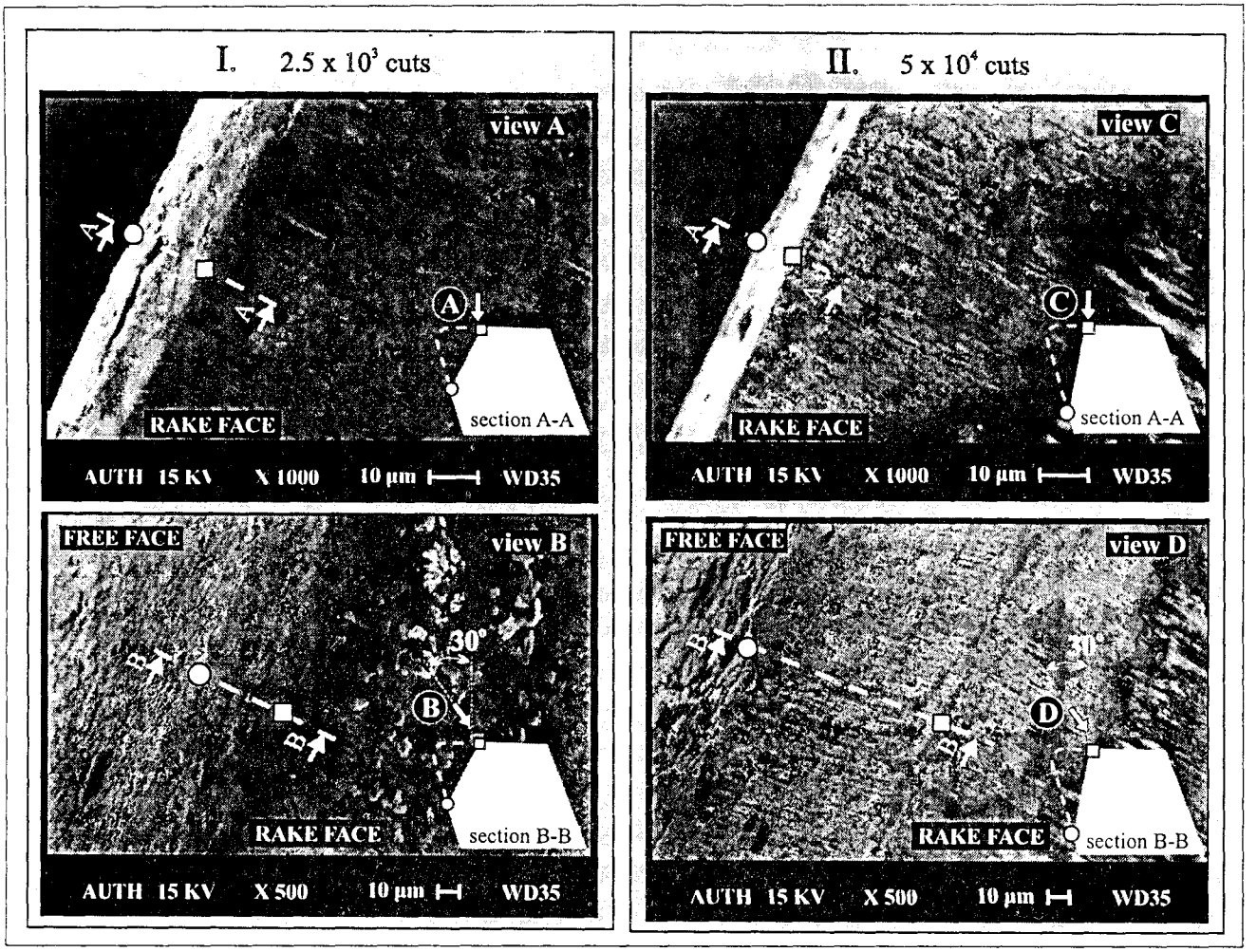

Fig. 9: Progress of the tip breakage of the cutting edge due to the accumulated number of cuts $\gamma=11.5°$, $\alpha=11°$, $\kappa=45°$, $b=5.67$ mm, $v=100$ m/min, tool P30, coating TiN, $t=4$ µm, workpiece 42CrMo4V, $R_m=105$ daN/mm²

ting herewith the unavailability of the whole insert. S ch a state implements the worsening of the workpiece material quality and the rising of the machining noise level.

The described wear progress of the tip of the cutting edge was measured versus the successive cuts number for various feedrates, and the corresponding results are penned in figure 10. In this diagram, the magnitude SV_{eff} is inserted for two of the used feedrates, illustrating the reduction of the projection of the broken chamfer and the corresponding increase of the wear of the free face.

7. THE PROGRESS OF THE COATING FAILURE ON THE RAKE FACE

Despite the early damage of the tip of the cutting edge, due to the high level of developed stresses, the coating kept its initial coherence on the rake face and continued successfully its operation, exhibiting a progressive cohesive failure. Although the failure appearance could be scanned optically, the most secure method to judge the coating status quantitatively is the EDX spectrography. The corresponding diagrams superficially to the inspected region offer the ratio of the scanned metals, and this information is adequate for the characterization of the coating condition. Typical results of such investigations are presented in figure 11. The inserted diagrams, in combination to the relative photographs illustrate the progress of the coating failure and its mode. In the first case the coating is undamaged since only its metallic Titanium component appears. In the middle diagram the coating has released its initial coherence and the Tungsten ground material becomes observable. The coexistence of coating and substrate material describes a typical cohesive failure mode, i.e. micro-chipping and not macro- delamination. Finally, the last EDX - micrograph combination illustrates a typical excessive coating failure. The only scanned elements fit to the structure of the cemented carbide substrate material. This insert status orients its operational limit, since its further utilization leads to improper superficial quality of the derived workpiece surface. Besides this, the abrasive wear of the cutting insert is accelerated.

Figure 12 illustrates the typical course of a specific insert cutting edge after the breakage of the cutting edge tip.

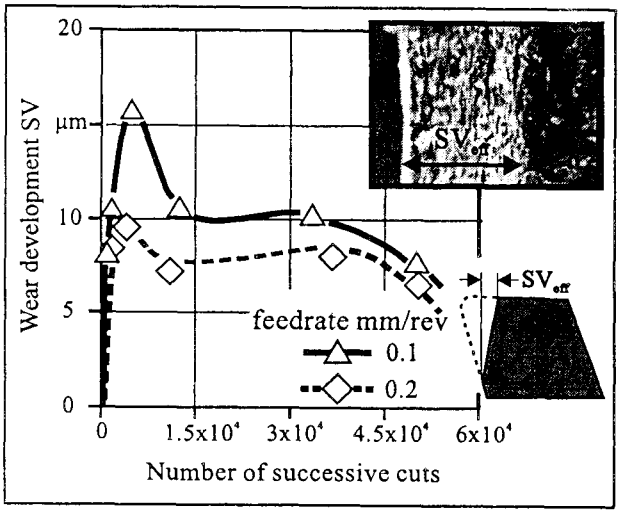

Fig.10: The progress of SV_{eff} versus the number of accumulated successive cuts $\gamma = 1\ I.5''$, $\alpha = 11''$, $\kappa = 45''$, $b = 5.67$ mm, $v = 100$ m/min, tool P30, coating TiN, $t = 4$ μm, workpiece 42CrMo4V, $Rm = 105$ daN/mm²

In the upper micrograph, after a significant number of successive cuts, the coating of the rake face remains undamaged, without any indications of decohesion. The EDX analyses verified this optically obtained result. Furthermore, the intermediary micrograph obtained after an advanced number of consecutive cuts illustrates the first indications of the coating internal coherence release. Finally, the lower micrograph exhibits a totally destroyed coating on the rake face. In the entirety of the investigated cases, after the failure of the tip of the cutting edge, the insert rake face exhibited quite better

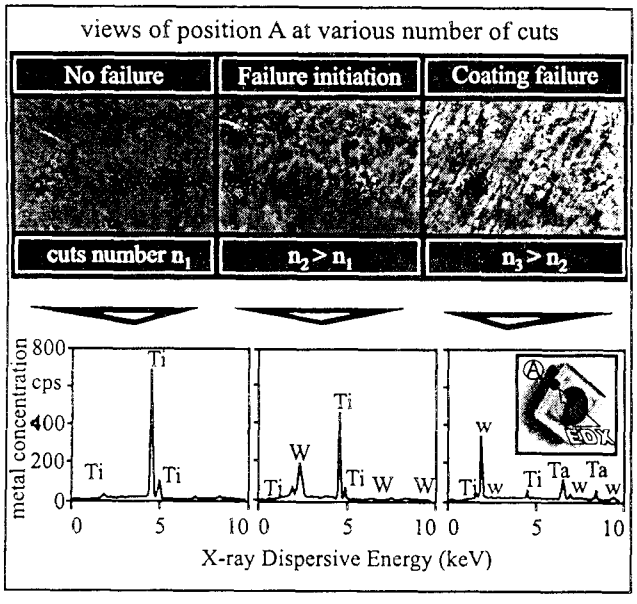

Fig.11: Determination of the coating fatigue failure progress through EDX micro- spectral analyses

behaviour at the higher feedrate than the corresponding at lower ones.

To computationally interpret this behaviour, the developed FEM model was adjusted to represent the cutting edge after its tip breakage. This modeling procedure and a typical solution result are illustrated in figure 13a. The created failure chamfer of the cutting edge was simulated and the model was solved for the maximum developed undeformed chip thickness of *128 μm*, occurring at the exit region of the tool from the workpiece and corresponding to feedrate *0.2 mm/rev*. As it can be seen from the

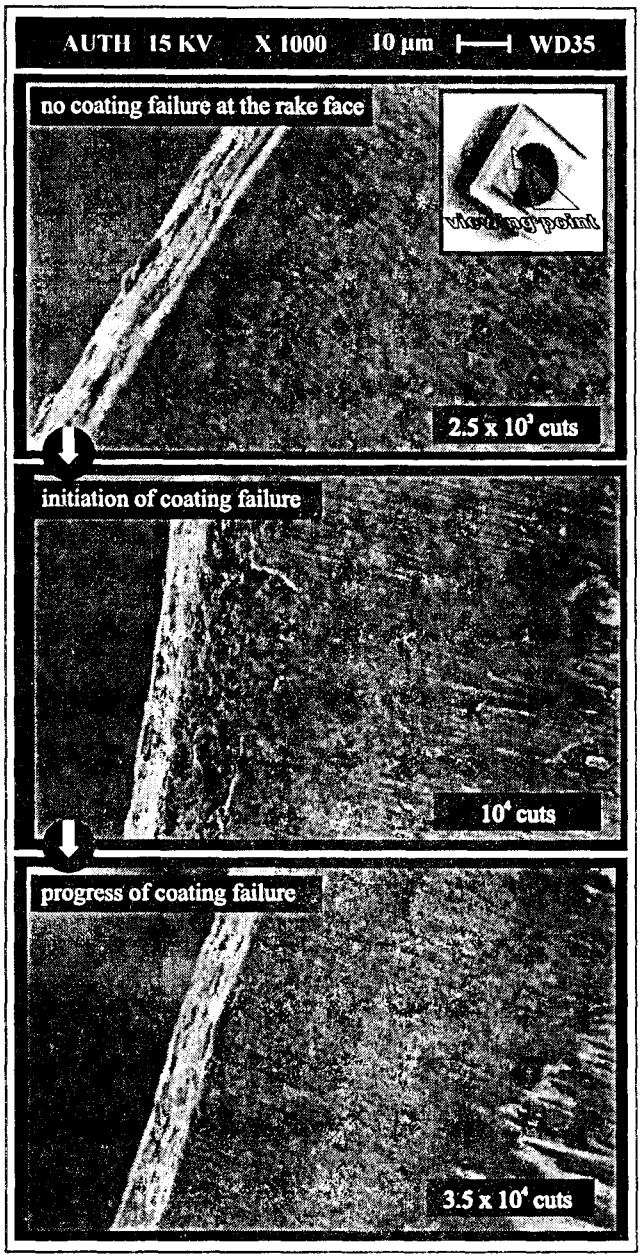

Fig.12: The course of the coating failure in various number of accumulated successive cuts $\gamma = 11.5''$, $\alpha = 11''$, $\kappa = 45''$, $f_z = 0.1$ mm/rev, $b = 5.67$ mm, $v = 100$ m/min, tool P30, coating TiN, $t = 4$ μm, workpiece 42CrMo4V, $R_m = 105$ daN/mm²

inserted stress contours, within the new geometry of the cutting edge, the maximum stresses occur at the new tip of the cutting edge, located besides the free face. This behaviour exhibits the progress of the formed chamfer, observed after the failure of the edge apex. On the other hand the stresses developed along the rake face, exhibit the fatigue failure potential of the superficial coating. The diagrams in the upper part of figure 13b state that the distributions of the von Mises equivalent stresses along the coated part of the rake face exhibit their maximum value always at the same position. Nevertheless, the maximum stress value depends on the undeformed chip thickness and this dependency is also shown in the middle diagram of figure 13b. Considering that every experiment was conducted at a constant cutting speed,

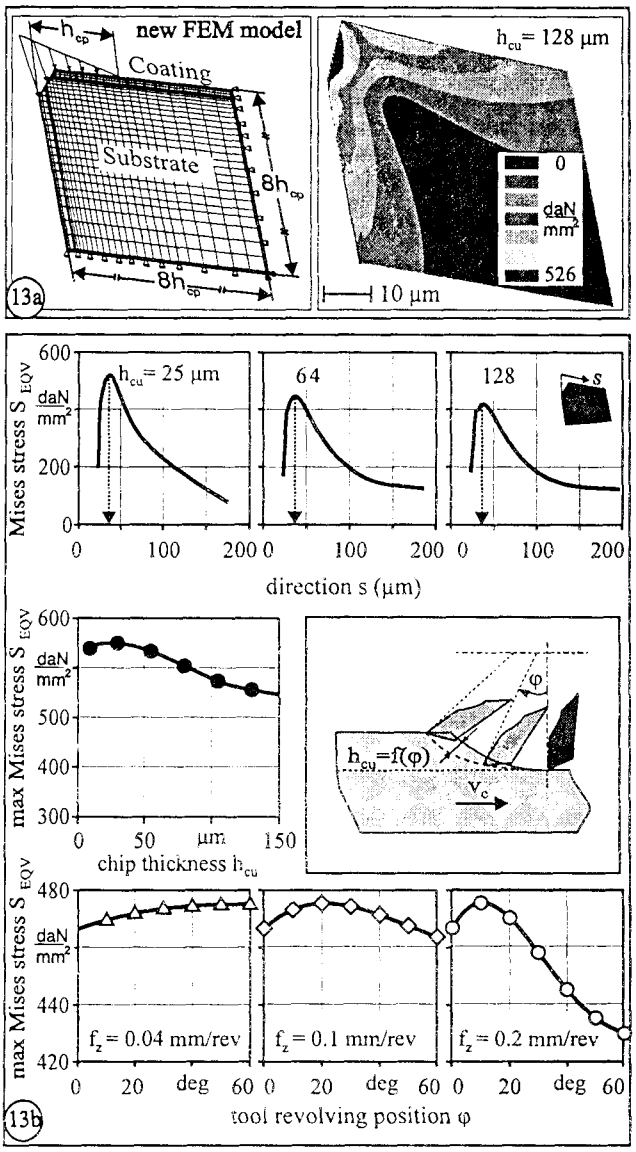

Fig.13 : The FEM interpretation of the coating fatigue failure progress on the rake face, in various feedrates g =11.5", a=11", x=45", b=5.67 mm, v=100 m/min, tool P30, coating TiN, t=4 wm, workpiece 42CrMo4V, Rm=105 daN/mm2

the time per tool revolution was kept unchanged for every utilized feedrate.

Taking into account the influence of the maximum stresses on the undeformed chip thickness, the course of the maximum coating stress versus the position of the cutting edge within the workpiece is presented in the bottom part of figure 13b. A yielding remark from these three diagrams, is that although for every feedrate the maximum coating von Mises stress is the same, the time that the coating remains at a high stress level is longer. This could be the reason for the better experimental behaviour that the coating exhibited at higher feedrates.

The experimental and the computational results are summarized in figure 14. In this illustration, the experimental observations for each used feedrate are inserted in the Woehler diagram of the used TiN coating. The coordinates for each point correspond to the achieved number of accumulated cuts and the developed stresses on the rake face. The experimental results are in good agreement with the corresponding computational ones.

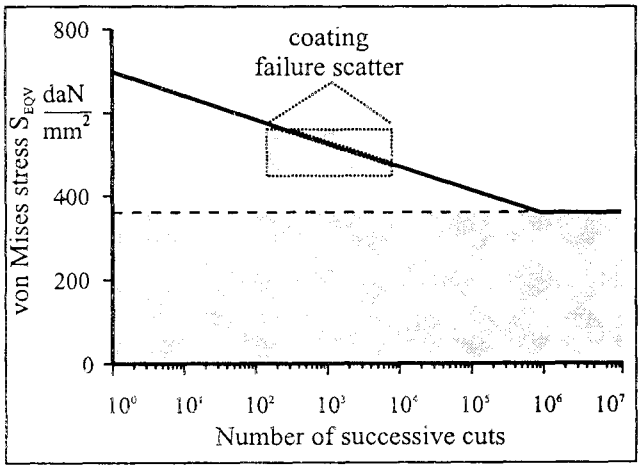

Fig.14: Comparison of the developed stresses during the milling process with their permitted values and explanation of the experimental results g =11.5", n=11", x=45", b=5.67 mm, v=100 m/min. tool P30, coating TiN, t=4 ,m, workpiece 42CrMo4V, Rm=105 daN/mm²

8. CONCLUSIONS

The experimental and computational results presented in this paper explain quantitatively the observed behaviour of coated cemented carbide inserts in milling of a hard workpiece material. The existing coating fatigue properties in combination with the stress reserves of carbide substrates can be used to predict the cutting performance of inserts, with the aid of experimentally derived technological data. Herewith, design parameters of the coated inserts can be modified and optimized, leading to the improvement of the whole cutting process.

REFERENCES

[1.] *Koenig. W., Fritsch, R., Kammermeier, G.*, 1992, **New Approaches to Characterizing the Performa.nce of Coated Cutting Tools**, Annals of the CIRP Vol. 41/1

[2.] *Bouzakis, K., D., Vidakis N.*, 1997, **Effect of mechanical stresses developed during gear hobbing on the fatigue failure of tool coatings**, Int. Jour. for Manufacturing Science and Production, vol.1:51-58

[3.] *Knotek, O., Bosserhoff, B., Schrey, A., Leyendecker, T., Lemmer, O., Esser, S.*,1992, **A new technique for testing the impact load of thin films: the coating impact test**, Surface and Coatings Technology, 54/55:102-107

[4.] *Bouzakis, K., D., Vidakis, N., Leyendecker, T., Erkens, G., Wenke, R.*, 1997, **Determination of the fatigue properties of multilayer PVD coatings on various substrates, based on the impact test and its FEM simulation**, ICMTF97, St. Diego, also in press in Int. Jour. Surface and Coatings Technology.

[5.] *Bouzakis, K., D., Vidakis, N., Leyendecker, T., Lemmer, O., Erkens, G., Esser, G.*, 1996, **Determination of the Fatigue Behaviour of Thin Hard Coatings Using the Impact Test and a FEM Simulation**, Surface and Coatings Technology 86-87:549-556.

[6.] *Vidakis, N.*,1997, **Determination of the fatigue strength of thin hard coatings for the prediction of their life time on hybrid bearings steel races, used in high speed spindles of machine tools**, Ph.D. Thesis, Aristoteles University of Thessaloniki, Greece.

[7.] *Bouzakis, K., D., Vidakis N.*, 1995, **An evaluation method of thin PVD films adhesion using the impact test and a FEM simulation of the contact response**, Tribology in Industry, Vol.3/95: 69-75.

[8.] *Bouzakis, K., D., Vidakis N.*,1996, **Prediction of the fatigue behaviour of PVD coatings in the Ball on Rod RCF Test, using an Elastic Plastic FEM simulation**, In press in WEAR (paper 7494).

[9.] *Bouzakis, K., D., Vidakis N.*, 1996, **Determination of plastic behavior of hard materials using the Rockwell B test and a FEM simulation**, proc. of the 2nd International Conference on Tribology Balkan-Trib96, Thessaloniki, Greece: 448-459

[10.] *Swanson Analysis System, INC.*, 1995, **"ANSYS user manuals"** Vol.l Theory, Vo1.2 Procedures, Vo1.3 Elements Vo1.4 Con ands

[11.] *Brooks, K.*, 1987, **Word directory and handbook of hardmetals**, 4th edition, international carbide data.

UDK 621.914.6:621.8.33

S. SEKULIĆ, S. VUKSANOVIĆ

Some Suggestion for Cutting Resistance Determination by Face Milling

With the aim to determine the cutting resistance components more precisely, a large investigations with one-tooth milling cutter were made, with the aim to register moment values for cutting resistance components. On the basis of profile for Fy and Fx components by transformation in cutting plane, the profiles of changes in tangential Ft and radial Fr cutting resistance components were obtained. The results obtained by processing with one-tooth-milling cutter can be used in real conditions, i.e. by processing with tools with many teeth, by superposition of profiles, obtained in one-tooth milling.

Keywords: face milling, cutting resistance components, one-tooth milling cutter, superposition of profiles

1. INTRODUCTION

In the literature there are many mathematically based models for theoretical determination of cutting resistance. The values for cutting resistance obtained by application of these models are different but useful for consideration of individual influences on cutting resistance. Previous results of cutting forces measurements using dynamometer showed that the description of mechanical models is simplified regarding a very complex milling process and that is the reason for the deviation between the calculated and measured values. So for the component Fz (perpendicular to cutting plane) a significant difference between measured and calculated values is obvious. In some cases by investigation of milling feed effects, the theoretical and experimental values for cutting resistant component Fz are even qualitatively not in accordance. The analysis showed the theoretical values for tangential component of cutting resistance, obtained from transformations based on elements of geometry of chip cross-section, to be in good accordance with experimental values. However, the derived equations for the calculation of vertical component did not provide even qualitative agreement, so it is obvious that in mathematical models some very important factors are not taken into account.

For the analysis of deformations of machine tool elements, cutting tool load, vibrations and their influence on the preciseness and the quality of the processed surface, the understanding of character of cutting resistance changes is necessary. The cutting forces in face milling has been extensively studied both analytically and empirically.

In analytical modeling approaches, theories of single-point oblique cutting, energy method, flow-stress method and single-shear plane method may be applied. In analysis of cutting process the differentiation should be made between the resistance acting on one tooth and the resistance acting on each tooth that is engaged with the workpiece. Especially interesting is the resistance in case of combined, upcut and downcut face milling.

In experimental investigations the cutting resistance components are measured in three orthogonal directions: in direction of feed motion (*Fy*) and perpendicular to the feed motion (*Fx*) in cutting plane as well as perpendicular to milling plane (*Fz*). The resultant resistance of measured values for the components *Fx*, *Fy* and *Fz* follows as $Fu=(Fx^2+Fy^2+Fz^2)^{1/2}$. The cutting resistance on one tooth in cutting plane may be decomposed into tangential acting on tooth top, tangential component (*Ft*) and perpendicular to the same direction, radial component (*Fr*). Total feed resistance is a vectorial sum of respective feed resistances of all teeth engaged with the workpiece.

Two characteristic values for the main cutting resistance per tooth are: maximal value Ft max and mean value *Ft m. Using Ftmax* values the maximal chip load, i.e. spindle load is analyzed, whereas *Ftm* value is used for calculation of required cutter power.

Prof. Dr Sava St. Sekulić, dipl. ing.
Sava A. Vuksanović
Institute of Industrial System Engineering,
Faculty of Technical Science, University of Novi Sad,
Novi Sad

2. AIM OF WORK

The aim of this work was to register and memorize the instantaneous values for cutting resistance components in enough short time intervals on the basis of experiments with face milling using one-tooth cutter. On the basis of measured values using transformation equations, the instantaneous values for tangential *Ft* and radial *Fr* components of cutting resistance, as well as total cutting resistance *Ft* should be determined.

By real cutting with many teeth engaged with the workpiece, the resultant component of cutting resistance should be determined applying the method of superposition.

3. EXPERIMENTAL INVESTIGATIONS

3.1. Conditions in experimental investigations

Workpiece material was constructial steel for the improvement Č.1730 (DIN C60), dimensions *200x100x100 mm*. According to JUS standard, the chemical composition is provided as follows: *0.61 C%; 0.22 Si%; 0.72 Mn%, 0.029 S%* and *0.014 P%* ; mechanical characteristics: tensile strenght of material $M=800\ MPa$ and hardness by Brinell $HB=241$.

Tests were made on vertical milling machine tool "Prvomajska" FSS GVK 3 with following characteristics: power of electromotor for primary and feed motion $P=14.5+2.2$ *(kW)*, rpm ranging from *28-1400* (18 degree), feedrate ranging from *16-800 mm/min* (18 degree).

End milling cutter "Jugoalat" G 715 125 mm with mechanically fixed cemented carbide inserts was used as a tool. Geometry characteristics of the tool are: teeth number $z=8$, tool cutting rage angle $\kappa=75^o$, tool normal rake $\gamma=7^o$, tool normal clearance $\alpha=18^o$. Square rotating cemented carbide insert, quality P25, were used as a tool material. During milling process the cutter was in symmetrical position related to the workpiece.

Cutting conditions included following widely ranging elements: cutting speed v between *1.83 and 4.65 (m/s)*, i.e. respective number of revolution n between *280* and *710 (o/min)*, feed per tooth sz between *0.142* and *0.351 (mm/t)*, i.e. respective feed rate s between *63* and *160 (mm/min)* and depth of cut between *0.67* and *3.37 (mm)*. The measurement of the elements of cutting resistance was performed using three-force-component dynamometer on piezoelelectric principle "Kistler" type 9257 A. In Fig 3.1. the scheme of complete installation for measurement and computer data acquisition is presented.

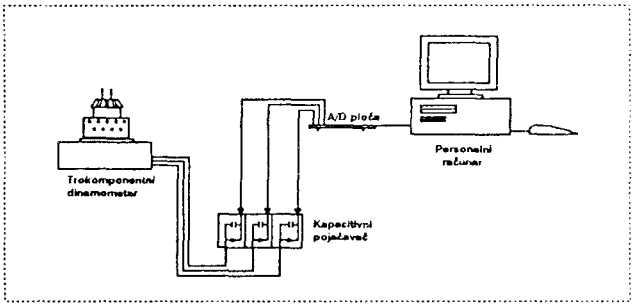

Fig 3.1

3.2. Result of measurements

The values of cutting resistance components, expressed by voltage signal at defined cutting condition, were fed into the data base. In order to obtain the cutting resistance values in [N], the calibration was performed. Based of ratio between voltage signals and units for cutting resistance in [N], data base was converted, using software "Excel 5", Microsoft. New data bases were processed applying "Easyplot" for graphical data presentation. As the final result, *30* profiles (one for each cutting condition) were obtained.

4. DETERMINATION OF TANGENTIAL AND RADIAL COMPONENT AND RESULTANT CUTTING RESISTANCE IN CUTTING PLANE

In milling process the understanding of tangential and radial component of resultant cutting resistance in cutting plane is of a special interest. Since the values of three components depend on the position of teeth engaged with the workpiece, their values must be known during interval of the tool and workpiece contact. Based of experiments profile of changes of cutting resistance components, in direction of feed motion *Fy* and perpendicular to the same direction in cutting plane *Fx* is known (Fig 4.1), it is possible by application of transformation equations

$$Ft(\varphi) = Fy(\varphi) \cdot \cos\varphi + Fx(\varphi) \cdot \sin\varphi\ ;$$

$$Fr(\varphi) = Fy(\varphi) \cdot \sin\varphi\ Fx(\varphi) \cdot \cos\varphi$$

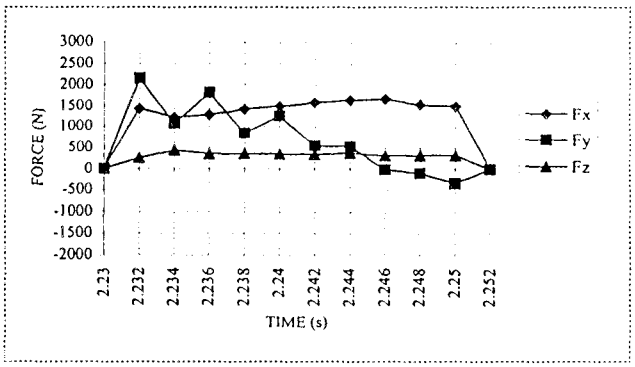

Fig. 4.1. Profile Fx, Fy i Fz

to obtain the profiles of tangential *Ft* and radial *Fr* cutting resistance components depending on the position of teeth engaged with the workpiece.

Precise procedure was conducted by acceptance of uniformly arranged points on the contact curve and for each position from profile *Fx* and *Fy*, using transformation equations, the respective profile *Ft* and *Fr* was obtained. An example for the mentioned procedure is presented for one arbitrary chosen work regime (item 16). Graphic interpretation of components of cutting resistance, depending on the position of teeth engaged with the workpiece is given in Fig.4.2., Fig.4.3., and Fig.4.4.

The values, tangential *Ft* and radial *Fr* component, the resultant cutting resistance *Fxy* (*Ftr*) in cutting plane and total cutting resistance, depending on the position of teeth engaged with the workpiece are given in Tab. T-3. for following cutting conditions $v=2.95$ *[m/s]*, $s_z=0.351$ *[mm/t]*, $\delta=1.50$ *[mm]*, $s=160$ *[mm/min]*.

In Fig.4.5. comparative profiles for components *Ft*, *Fr* and *Fu* ($Fu=(Ft^2+ Fr^2 Fz^2)^{1/2}$) are presented. From Tab.3., column for *Fr*, it is obvious that the component changes sign at angle $\varphi \neq 0$, i.e. between position 7-8, which also can be seen in Fig.4.5. (profile *Fr*).

5. COMPONENTS OF CUTTING RESISTANCE BY MANY TEETH ENGAGED WITH THE WORKPIECE

In order to determine the values of tangential and radial components of cutting resistance by real milling, which are related to the greater number of engaged teeth, the method of repetition and superposition was applied. For this purpose the cutting with 1, 4, 6, 8, 12 and 14 teeth was taken into consideration. The superposition method is in fact a periodical repetition of profiles of tangential, radial and vertical component of cutting resistance, whereby the repetition frequency is determined on the basis of intervals, which result from the ratio of work angle, defined from workpiece width, cutter radius and angle between two neighboring teeth *360/z*.

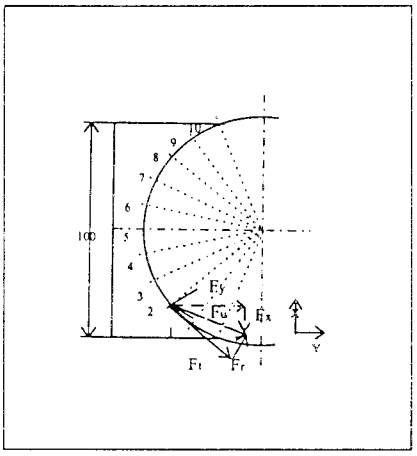

Fig. 4.2

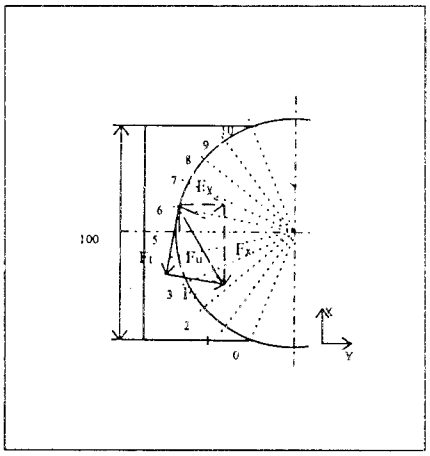

Fig. 4.3

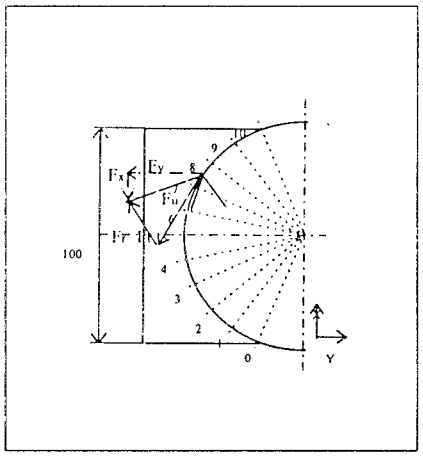

Fig. 4.3

Tab. T-3.

i	Fx [N]	Fy [N]	Fz [N]	φ	Ft [N]	Fr [N]	Fxy [N]	Fu [N]
1	-1424.23	2148.78	253.99	42.504	2501.79	621.87	2577.92	2590.40
2	-1220.77	1066.10	432.85	31.878	1599.67	260.60.	1620.76	1677.56
3	-1280.61	1817.35	350.40	21.252	1852.26	1229.57	2223.21	2250.65
4	-1424.23	839.62	357.71	10.626	1554.63	562.60	1653.30	1691.55
5	-1496.04	1248.39	352.40	0.000	1496.04	1248.39	1948.49	1980.10
6	-1587.80	546.86	339.10	-10.626	1459.73	830.27	1679.34	1730.23
7	-1641.65	535.81	367.69	-21.252	1335.79	1094.43	1726.88	1765.59
8	-1677.56	-22.10	312.50	-31.878	1436.21	-867.18	1677.70	1706.55
9	-1539.92	-99.43	319.15	-42.504	1202.45	-967.13	1543.13	1575.79
10	-1498.03	-342.48	321.15	-53.130	1172.80	-992.94	1536.38	1569.59

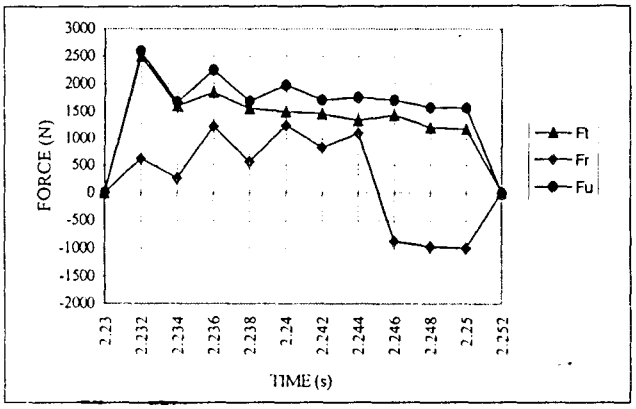

Fig. 4.5. Profile Ft, Fr i Fu

As:

$$\sin\frac{\Phi}{2} = \frac{\frac{B}{2}}{\frac{D}{2}} = \frac{B}{D} = \frac{100}{125} = 0.8$$

so the cutting angle is:

$$\Phi = 2\cdot\left(\arcsin\frac{B}{D}\right) = 106.26$$

Thus the number of engaged teeth is:

$$z_u = \frac{L}{D\cdot\pi} = \frac{\Phi}{360\,/z}$$

Superposition is semigraphic, since it was performed by arithmetical summarizing of values for overlap profiles corresponding to the position of teeth determined from the main profile, defined tabular at time intervals of 0.002 sec. Based on the mentioned above the graphical presentations were obtained, which correspond to the mentioned tooth number. By periodical omission, the tooth numbers 2, 3, 5 and 7 by cutter with 4, 6, 8, 10 and 14 teeth (by overlap of each second, pair profile) can also be considered. In Fig.4.6. graphical presentation of superponed tangential, radial and vertical components of cutting resistance for each component separately and the total resistance are given for $z=1$ and $z=6$.

6. CONCLUSIONS

On the basis of the mentioned above following conclusions can be made:

- proposed methodology for the determination of instantaneous values of tangential Ft and radial Fr cutting resistance component, by transformation component profiles Fxy and Ftr, based on the common time intervals of tooth position, enables a precise profile transformation
- based on instantaneous values of Ft and Fr components of all teeth engaged, total cutting resistances in interesting direction in cutting plane (Fx,Fy) can be determined.
- the analysis of diagram of dependence of changes in tangential Ft, radial Fr and vertical Fz cutting resistance component in function of tooth number engaged with the workpiece, indicates that the component Fr changes sign, so the upcut milling is transformed in downcut milling at $\varphi \neq 0$ $(\varphi < 0)$.

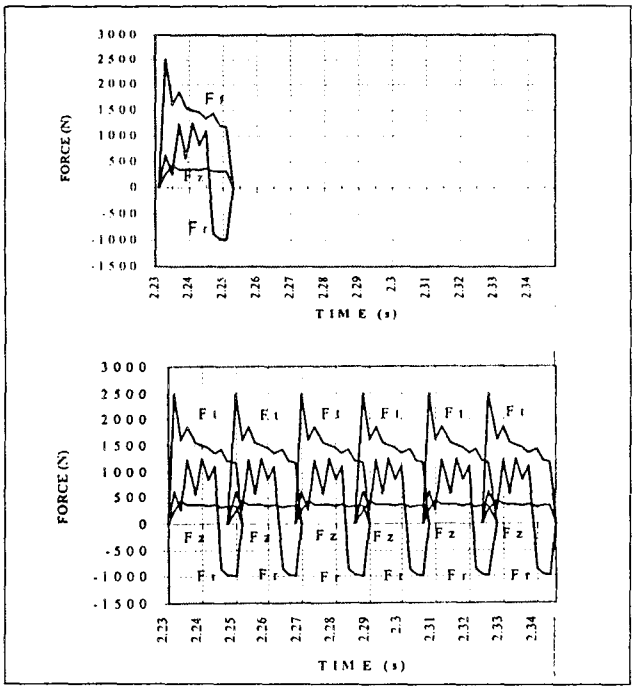

Fig. 4.6. z=1 i z=6

LITERATURE

[1.] *Fu, H. J., De Vor, R.E., Kapoor, S. G.*: **A Mechanistic Model for the Prediction Of the Force Systems In Face Milling Operations**, Jour nal of Eng. for Ind. Vol. 106/81, 1984.

[2.] *Kamm,H.*: **Beitrag zur Optimierung des Messerkopffräsens**, Dissertation, Universität, Karls1977.

[3.] *Kronenberg, M.*: **Grudzuge der Zerspanungslehre**, Springer-Verlag, Berlin, 1954.

[4.] *Rozhong, Z., Wang, K. K.*: **Modeling of Cutting Forces Pulsation in Face Milling**, Annals of CIRP, Vol.32/1/1983.

[5.] *Aoyaina, H., Ohzeki, A., Mashine, A., Takashita, J.*: **Cutting Force Sensing in Milling Process**, VDI BERIHTE Nr. 1179, 1995, pp 319-333.

UDK 621.9:531.43

G. PETROPOULOS, H. KARAHALIOU

RESEARCH

Testing The Homogeneity of The Roughness of Surfaces Generated By Face Turning Operations

The overall variability of face turned surfaces is investigated regarding surface roughness as criterion. The versions of face turning performed were in-feed and out-feed turning. Statistical distributions of the standardized roughness parameters, R_a and R_m values obtained by appropriate application of the x^2-test show that under constant cutting speed Gauss distribution is followed, while under maximum cutting speed there appears significant deviation from normality with positive skewness. The homogeneity of surface roughness is investigated statistically by a two-way classification analysis of variance applied to the experimental data. The test surfaces were divided in annulars and circular sectors and in general a highly significant annular effect has been found, whereas insignificant variation is detected among sectors. The establishment of these results can contribute to the quality control of turned surfaces providing a guide to cites selection for representative surface roughness measurements in accordance with the estimation of their tribological behaviour.

Keywords: turning operations, surface roughness, variability

1. INTRODUCTION

Turning operations are widely established in machine shop industry. The majority of research works focused on turning process, among others, investigate the cutting mechanisms and the machinability parameters, as well as their interdependence.

Surface roughness constitutes an essential dependent variable in cutting processes, inasmuch as its knowledge or prediction is critical to design and manufacture of operational surfaces (mating and free). In consequence, surface roughness of components has strong influence on their tribological behaviour and performance. Further, special knowledge and analysis of roughness are effective in problems of simulation, optimisation, adaptive control, development of data bases etc [1-10].

The surface roughness values are dependent upon various variables and parameters. The variation of roughness for any cutting system considered (cutting process-machine tool-cutting tool- workpiece) is due to a) experimental error b) progressive tool wear c) vibrations of the cutting system (chatter) and d) to the degree of replication of experimental results [11 -14].

Georgios Petropoulos,
Department of Mechanical and Industrial Engineering,
University of Thessaly, Greece
Hariclia Karahaliou,
Department of Mechanical Engineering,
Aristotle University of Thessaloniki, Greece

It is well known that measured values of magnitudes, which characterize the roughness of turned surfaces, mainly the standardised R_a (CLA value) and peak-to-valley R_{max} parameters, present a significant amount of scatter, something that gives roughness a stochastic character [20-22]. Therefore, modelling of statistical distributions relevant to these parameters, appears to be of great interest for carrying out various statistical tests, as well as for quality control purposes [16, 18]. A related task is the statistical testing of the homogeneity of the turned surface regarding the distribution of its roughness. This procedure can help to the location at any case of the positions and directions for representative measurements on the surface (usually the sample size for these measurements must be sufficiently large) which are not incorporated in the relevant standards, as well as to the estimation and prediction of its tribological behaviour.

Previous investigations regarding the variability and the homogeneity of roughness values of technological surfaces machined by longitudinal turning are limited and conflicted, while there is lack of information about face turning (facing) operations.

In view of literature it is argued that standard surface roughness parameters R_a, R_{max}, R_q obtained in conventional turning with sharp tool [15, 23], as well as with progressively wearing tool, conform to the Gauss distribution [1,16,18]. On the contrary, it has been supported that surface roughness does not follow the Gauss distri-

bution [12]. In a recent paper of the authors [25] it is shown that the R_a values in most of the cases considered follow the Gauss distribution at *99 per cent* significance level, while in all cases considered the log-normal distribution is obeyed at *95 per cent* significance level.

It has also been supported that there is statistically significant homogeneity according roughness of surfaces machined by oblique external longitudinal turning [17], whereas the homogeneity or not in facing is not yet been investigated.

The present work is aimed at the investigation of the overall variability of quasi steady state external single point oblique face turning operations considering surface roughness, incorporating the modelling of the statistical distributions of roughness parameters over the machined surfaces and testing the homogeneity of surfaces regarding their roughness as a criterion.

Facing exhibits different kinematics than longitudinal turning, as cutting speed varies linearly with workpiece instant diameter for constant spindle rotational frequency for either of its two versions, namely, in-feed face turning (IFT) and out-feed face turning (OFT). This characteristic of cutting speed deceleration or acceleration respectively, affects shear strain velocity, chip formation and morphology and chip interface temperatures in a different manner than in longitudinal turning with subsequent effects on the cutting dependent variables and machinability parameters.

2. EXPERINIENTAL PROCEDURE

2.1 Instrumentation

The necessary experiments were carried out in two lathes of fairly good operational condition and of the following technical specifications :

	Lathe A	Lathe B
Nominal power, kW	10.0	7.5
Maximum distance between centers, mm	2 000	1 500
Swing-over bed, mm	280	210

The surface roughness measurements were carried out on a stylus type profilometer Talysurf model 4 with wavelength cut-off of *0.8 mm* (typical for turned surfaces). To characterize roughness the R_a and R_{max} parameters were calculated. The stylus was moving in a direction perpendicular to the direction of the cutting speed for the measurement of R_{ar} and R_{max} (radial roughness in facing) and in tangential direction to measure R_{at} (tangential roughness in facing).

2.2 Cutting tool - Workpiece

As cutting tool a sintered carbide insert SANDVIK/ Coromant S6 equivalent to ISO P40 was employed properly clamped on a suitable standard tool holder with the following combined geometry:

Rake angle:	$\gamma = +6^o$
Tool side cutting angle:	$\kappa = 75^o$
Relief angle:	$\alpha = 11^o$
Tool approach angle:	$\kappa_1 = 15^o$
Inclination angle:	$\lambda_s = 0^o$
Cutting edge radius:	$r_e = 0.8\ mm$

The cutting tool was kept sharp during the experimental work.

The workpiece material was a plain medium carbon steel Ck60 in the form of bars of diameters *160 mm* and *300 mm*.

In all tests dry cutting was employed.

3. RESULTS AND DISCUSSION

In face turning operations the machined surface will exhibit obviously intense inhomogeneity compared to a relevant surface produced by longitudinal turning, owing to the cutting speed characteristic of the former, as already mentioned.

This fact stimulated us to statistically designed experiments in order to enable modelling of the statistical distributions of the standardized surface roughness parameters and on the other hand, to detect possible surface roughness variations (considering R_a and R_{max} values). For this purpose each machined surface was divided in annular rings (according to the size of the surface) and circular sectors and a two way classification analysis of variance was carried out. The cylindrical workpieces used had maximum diameters $D_1 = 160\ mm$, and $D_2 = 300\ mm$ respectively, and they were machined in separate lathes (B, A correspondingly).

a) Workpiece of maximum diameter $D_1 = 160$ mm:

The machined surface each time is divided in *3* concentric rings of the same thickness with center diameters *140 mm, 100 mm* and *60 mm* and in *4* continuous circular sectors by *90°*. A series of experiments of IFT is conducted under constant average cutting speed values *60, 100* and *185 m/min* and with radial feed rates *0.16, 0.25* and *0.46 mm/rev*. In every quadrant of each ring the radial roughness R_{ar} *(N=5)* and R_{max} *(N=1)*, as well as the tangential roughness R_{at} *(N=3)* are measured. Especially for the speed $v = 100$ *m/min* two replicates were taken.

b) Workpiece of maximum diameter $D_2 = 300$ mm:

Each machined surface is divided in *6* concentric rings of the same thickness and in *6* continuous circular sectors by *60°*. In each ring are measured $N = 18$ values of magni-

tudes R_{ar}, R_{at} at random positions, whereas in every circular sector randomly again $N = 10$ values of R_{ar} are measured. IFT and OFT are executed with maximum cutting speed $v_0 = 157$ *m/min* and radial feed rate sr *0.175 mm/rev.*

3.1 Modelling of the statistical distributions of roughness on the face turned surface

a) Workpiece of maximum diameter 160 mm:

The x^2-test of significance of goodness of fit on distributions ofthe measured values R_{ar} *(N=60)* and R_{at} *(N=36)* over the whole face turned surface is carried out for combinations of the maximum cutting speed and radial feed values (v_0, s_r).

The corresponding results are presented in Table 1 and Table 2. It is obvious that under constant cutting speed v_m in each of the three center diameters of the three annulars on the face turned surface, the relevant statistical distributions for combinations of the cutting conditions v_m and s_r conform to the Gauss distribution at *95 per cent* significance level.

Table 1. Results of the x^2-test application over the R_{ar} measured values in IFT under constant cutting speed per annular with center diameter (140-100- 60) mm

U_m m/min	s_r mm/rev	N	$\bar{R}_{ar}$	$\bar{S}_{Rar}$	d.o.f v	$x^2=\sum_{i=1}^{K}(f_i-f_{a1})^2/f_i$
60	0.16	60	2.4	0.17	6	12.1*
60	0.25	60	3.7	0.31	6	11.3*
60	0.46	60	7.9	0.21	5	3.2*
100	0.16	120	1.4	0.14	7	2.6*
100	0.25	120	3.6	0.13	7	4.8*
100	0.46	120	7.8	0.19	7	5.5*
185	0.16	60	1.3	0.11	5	4.1*
185	0.25	60	3.3	0.09	5	7.0*
185	0.46	60	8.1	0.20	5	6.3*

*Significance level 95%

Relative frequency versus R_{ar} *(N=120)* and R_{at} *(N=36)* values in form of histograms is plotted in Figure 1 under cutting conditions $v_m = 100$ *m/min* and $s_r = 0.16$ *mm/rev.* The relative theoretical curves are also plotted (full lines) with their characteristic parameters, namely, mean value R_a and standard deviation estimator s_{ra}.

Consequently, a similar statistical law is followed with the surface roughness distributions in longitudinal turning, which can be ascribed to the average cutting speed kept constant over the annulars under consideration. In this way, the facing operation applied presented almost same kinematics with longitudinal turning, something which can be achieved, in a wide range of combinations of cutting speed and workpiece diameter values, in modern lathes supplied by devices that maintain constant cutting speed in facing operations (C.N.C. lathes mostly).

Table 2. Results of the x^2-test application on the R_{at} measured values in IFT under constant cutting speed per annular with center diameter (140-100- 60) mm

U_m m/min	s_r mm/rev	N	$\bar{R}_{ar}$	$\bar{S}_{Rar}$	d.o.f v	$x^2=\sum_{i=1}^{K}(f_i-f_{a1})^2/f_i$
60	0.16	36	1.56	0.23	4	7.3*
60	0.25	36	1.50	0.28	4	8.2*
60	0.46	36	1.25	0.22	4	8.0*
100	0.16	36	0.80	0.18	4	6.8*
100	0.25	36	0.60	0.11	4	2.0*
100	0.46	36	0.58	0.12	4	6.0*
185	0.16	36	0.26	0.08	4	3.3*
185	0.25	36	0.38	0.14	4	4.3*
185	0.46	36	0.40	0.11	4	0.6*

*Significance level 95%

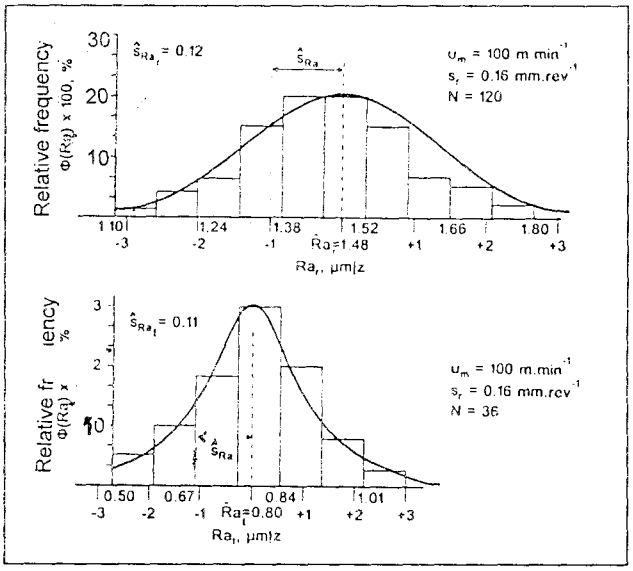

Figure 1. Histograms of the relative frequency of R_{ar} and R_{at} values and the relev nt normal theoretical curve

b) Workpiece of maximum diameter 300 mm:

The application of the x^2-test upon the observed R_{ar} and R_{at} roughness values of the specimen's surface machined by IFT and OFT under maximum cutting speed $v_0 = 57$ *m/min* has shown that the statistical distribution of the aforementioned surface roughness parameters for both facing versions deviates markedly from normality exhibiting positive skewness, that is pronounced relative frequency values to the left (Figures 2, 3).

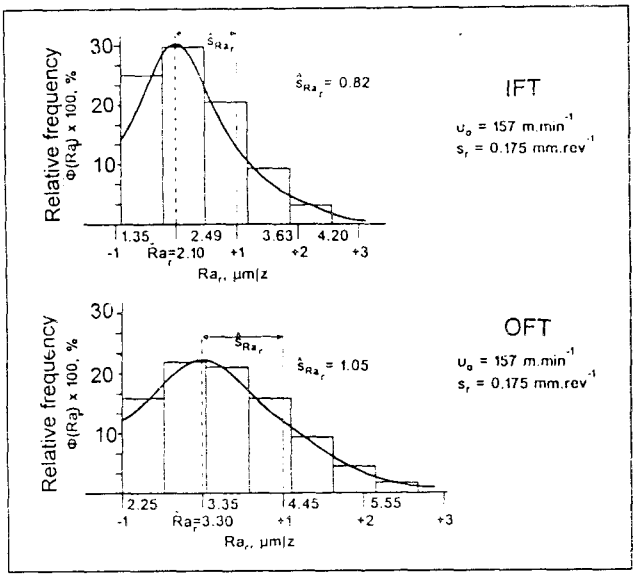

Figure 2. Histogr uns of the relative frequencv of R_{ar} values

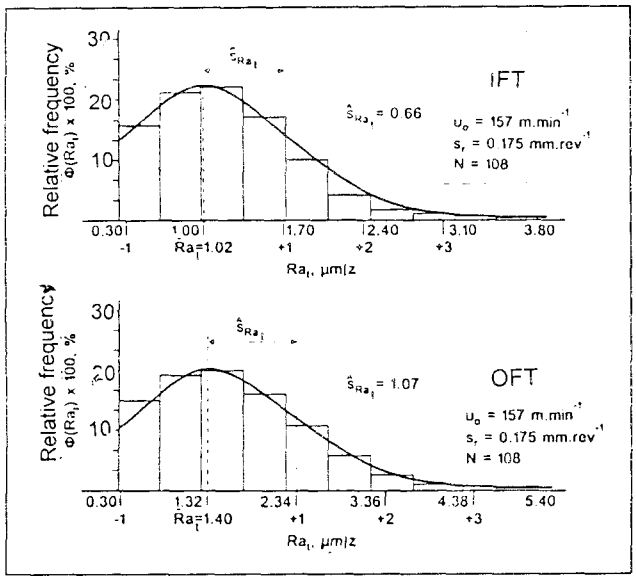

Figure 3. Histograms of the relative frequency of R_{at} values and the relevant thenrPrical curve

This fact can be attributed to increased probability for smaller values of roughness owing to the relatively small area of the surface, where cutting speed takes low values, due to built-up edge or discontinuous chip fonnation with subsequent roughness deterioration.

3.2 Testing the homogeneity of face turned surfaces

a) Workpiece of maximum diameter 160 mm:

In the direction of the representation and the statistical control of the homogeneity of the machined surface regarding its roughness as criterion, a two way classification analysis of variance is applied for all cutting conditions and all three roughness magnitudes, (R_{ar}, R_{at}, R_{maxr}) in order to detect any existing differences between the roughness values in the rings, as well as among the sectors.

Indicatively, in Table 3 the results of the analysis of variance are presented for the R_{ar}, R_{at}, R_{maxr} parameters of the surface machined with v_m=*60 m/min* and s_r=*0.16 mm/rev.*

Table 3. Two-way classification analysis of variance upon the roughness characteristics of a face turned surface (v_m=60 m/min, s_r=0.16 mm/rev)

Roughness	Variation	d.o.f. v	Mean variation	F	$F_{0.95}$
R_{ar}	Ur=0.45	3	s^2r=0.015	1.93	4.76($\beta.\varepsilon$ 3-6)
	Uc=1.74	2	s^2c=0.869	111	5.4($\beta.\varepsilon$ 2-6)
	Uc=0.05	6	s^2e=0.008	-	-
R_{af}	Ur=0.012	3	s^2r=0.004	0.63	4.76($\beta.\varepsilon$ 3-6)
	Uc=0.27	2	s^2c=0.136	21.2	5.14($\beta.\varepsilon$ 2-6)
	Uc=0.038	6	s^2e=0.006	-	-
R_{maxr}	Ur=2.25	3	s^2r=0.751	0.42	4.76($\beta.\varepsilon$ 3-6)
	Uc=18.2	2	s^2c=9.111	5.2	5.14($\beta.\varepsilon$ 3-6)
	Uc=10.5	6	s^2e=1.750	-	-

Ur=Variation in sectors; Uc=Variation in annulars; Ue=Residual variation

In general, all the numerical results of the applied two way analysis of variance for all the combinations of v_m and s_r in face turrting are qualitatively similar and the following conclusions can be drawn:

a) Workpiece of maximum diameter 160 mm:

For all the cases of face turning considered there insignificant difference of values R_{ar}, R_{at} *and* R_{maxr} between the circular sectors at *95%* significance level, while there is significant difference among rings, as it is expected due to process kinematics.

b) Workpiece of maximum diameter 300 mm:

Topographic diagrams of R_{ar} values for both facing versions are illustrated in Figure 4 and Figure 5.

1) First, a single analysis of variance is caried out on the roughness values R_{ar}, R_{at} between various annulars, as well as between sectors for both versions of facing(IFT, OFT). With the aid of this analysis it can be concluded that a signifcant difference appears at *95%* significance level in the R_{ar} and R_{at} values between rings, while on the contrary, unimportant difference is located in the R_{ar} values among sectors. This conclusion is valid for both facing versions.

2) By application of single analysis of variance in the total number of R_{ar} and R_{at} measured values between both facing versions it arises that insignificant difference ap-

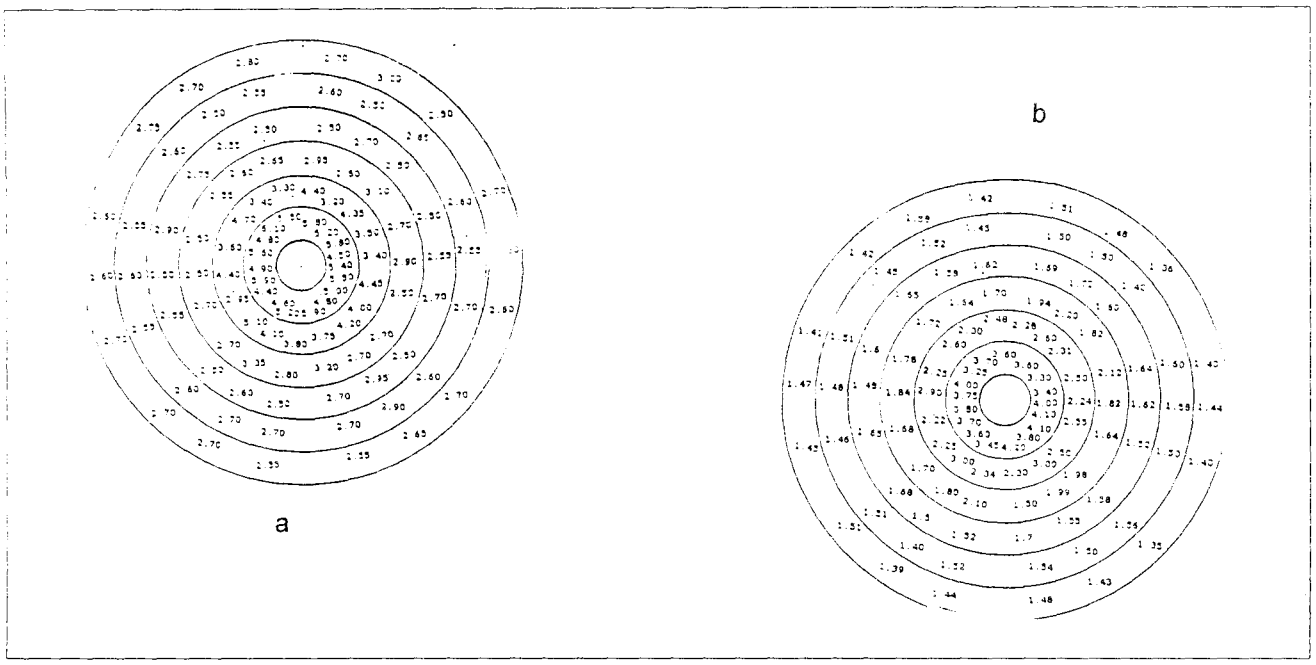

Figure 4: Topographic diagram of radial surface roughness R_{ar} over the annulars in a) OFT b) IFT

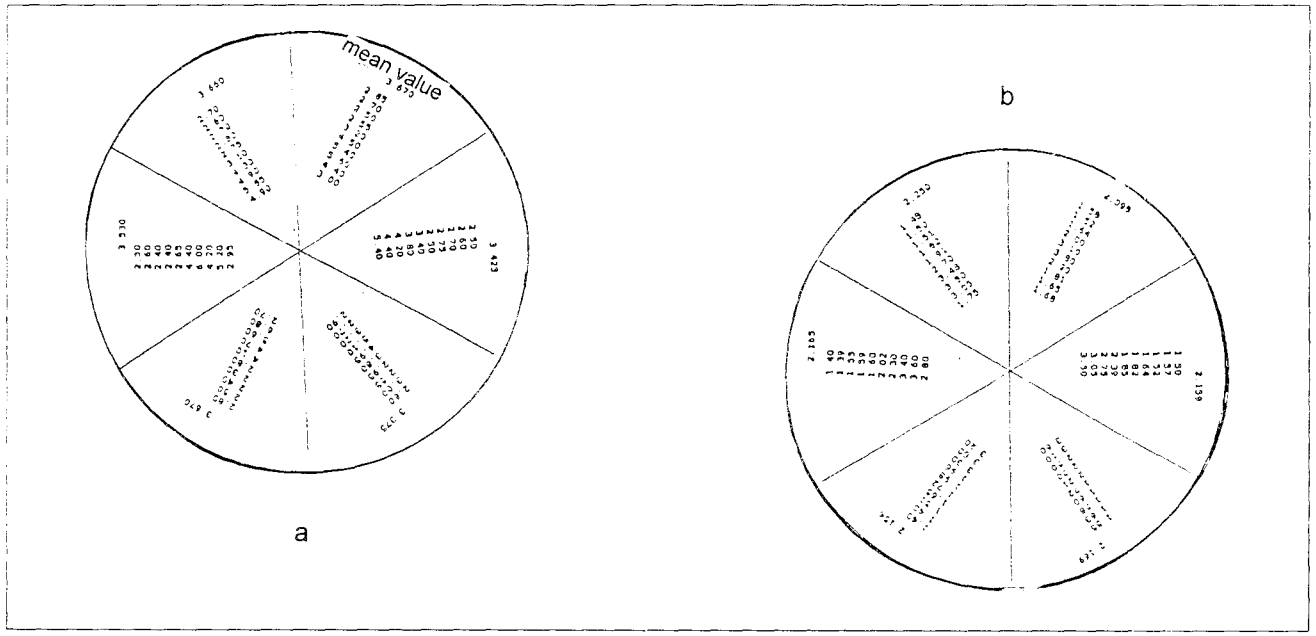

Figure 5. Topographic diagram of radial surface roughness R_{ar} over the sectors in a) OFT b) IFT

pears, respectively, at *95%* significance level. This means that the two surfaces machined by the two types of facing (IFT, OFT) do not exhibit any sigificant difference concerning their overall mean value of surface roughness.

3) By expansion of the application of single analysis of variance in the R_{ar} and R_{at} values of corresponding annulars, just as in relevant sectors for both types of facing, the numerical results obtained lead to the following conclusions:

- In both IFT and OFT in the inner annulars surface roughness is deteriorated because of built-up edge formation.
- There appears an important difference at *95%* significance level in the surface roughness magnitudes under study R_{ar} and R_{at} between relevant annulars machined by IFT and OFT face turning operations with the OFT values being higher, a fact that can be attributed to the different conditions of chip formation and chip interface temperatures risen, under the accelerated and the decelerated operation correspondingly. This item is in our opinion still open to study.

On the contrary, there is negligible difference in the R_{ar} values of relevant sectors for the two versions of facing applied. Taking into account that the surface roughness values of a circular sector constitute a representative sample of the roughness of the total surface, the aforementioned onclusion confirms the latter (number 2)

4. CONCLUSIONS

The most important conclusions from the present e nerimental-analytical work are,as follows:

1. As regards with modelling of surface roughness statistical distributions in face turning

- In facing under conditions of constant cutting speed the values of R_{ar} and R_{at} parameters follow the Gauss distribution at *95 per cent* significance level:

In both facing modes with constant maximum cutting speed the R_{ar} and R_{at} values deviate merkedly from the normal distribution presenting positive skewness, that means increased probability for the parameters considered to take smaller values.

2. Considering homogeneity of face turned surfaces with roughness as criterion

- On the machined surface under constant speed there appears insignificant difference of the R_{an} R_{ab} R_{maxr} values among the sectors at *95 per cent* sigxiificance level, whereas there is strong variation of the parameters values among annulars.
- On the machined surface under maximum cutting speed a significant difference of the R_{ar} and R_{at} values is detected among annulars at *95 per cent* significance level, while no difference is found for the Rar values over the sectors. This conclusion is valid for both facing versions namely, in-feed turning (IFT) and out-feed turning (OFT).

3. Summarizing, the establishment of the results of such statistical investigations can seriously contribute to the quality control of turned surfaces providing a guide for selecting cites for representative surface roughness measurements in practice, as well as to the estimation of their tribological behaviour.

REFERENCES

[1.] *Allen, A. F. and Brewer, R. C.*, **The Influence of Machine Tool Variability and Tool Flank Wear on Surface Texture**, Proc. Int. Mach. Tool Des. Res. Conf., Pergamon Press, Oxford, 1965, 301-314.

[2.] *Cook, N. H.*, **Manufacturing Analysis**, (Mass. Addition Readings), 1966

[3.] *Allgaier, E.*, **Die Oberflächengütte beim Drehen**, Werstattstechnik, 52, 1962, 155

[4.] *Brewer, R. C.*, **Parameter Selection Problem in Machining**, Arm. CIRP, 1966, 14-15

[5.] *Lambert, H. J.*, **Two Years of Finish Turning**, Research at the Technological University of Delft, Ann. CIRP, 10, 1962, 246

[6.] *Shaw, M. C. and Dirke, O.*, **On the Wear of Cutting Tools**, Microtechnic, 10, 1956, 187

[7.] *Solaya, V.*, **Wear of Carbide Tools and Surface Finish Generated in Finish Turning of Steel**, Wear, 2, 1959, 40

[8.] *Petropoulos, G. and Karahaliou, H.*, **Experimental Study and Stochastic Modelling of Cutting Forces in Face Turning of Steel with Sintered Carbide as Cutting Tool**, Technica Chronica, 13, 3, 1993, 45-70 (in Greek)

[9.] *Petropoulos, G. and Karahaliou, H.*, **A Phenomenological Experimental Analytical Research of Cutting Forces in Longitudinal and Face Turning Comparative Study and Stochastic Modelling**, Technica Chronica, 13, 4, 1993.

[10.] *Petropoulos, G. and Karahaliou, H.*, **On the Prediction of Tool Wear in Face and Longitudinal Turning Operations of Steel with Sintered Carbide Tools and Related Comparisons**, BALKANTRIB'93, Sofia, 116-126

[11.] *Albrecht, A. B.*, **How to Secure Desired Surface Finish in Turning Operations**, Am. Mach.,1956

[12.] *Jones, P. E.*, **The Accuracy of Surface Roughness Assessment**, Microtechnic, 17, 4.1963, 127

[13.] *Pekelharing, A. J.*, **Finish Turning**, Microtecnic 14, 1960, 61

[14.] *Pekelharing, A. G. and Schuermann, R. A.*, **Der Verschleiss und der Nebenschneide von Hartmetalldrehmeisseln und die Erzengte Oberflächenrauheit**, Werkstattstechnik, 45, 1955, 43

[15.] *Olsen, K. V.*, **Surface Roughness as a Function of Cutting in Finish Turning of Steel**, Am.Soc.Tool Manufact. Engrs, Technical Paper, 655, 1964.

[16.] *Petropoulos, P. G.*, **Statistical Basis for Surface Roughness Assessment in Oblique Finish Turning of Steel Components**, Int. J. Prod. Res., 12, 3, 1974, 345-360

[17.] *Petropoulos, P. G.*, **A Note on the Homogeneity of the Roughness on Oblique Finish Turned Surfaces**, Wear, 24, 1973, 147-152

[18.] *Sundaram, R. M. and Lambert, B. K.*, **Surface Roughness Variability of AISI 4140 Steel in Fine Turning Using Carbide Tools**, Int. J. Prod. Res., 17, 1979, 249-258

[19.] *Karahaliou, H. and Petropoulos, G.*, **A Stochastic Approach for Basic Machinability Parameters Modelling in Oblique Turning Operations**, Proc. 2nd Balcan Conf. on Operational Research, Thessaloniki, Greece, 1993, 840-855

[20.] **British Standards Institution**, Centre-Line Average Height Method for the Assessment of Surface Texture, B.5. 1134, 1961

[21.] **American Standards Association**, Surface Texture. ASA B 46, 1., 1962

[22.] *Olsen, K. V.*, **On the Standardization of Surface Roughness Measurements**, Bruel and Kjaer, Technical Review, 3, 1961, 3-32

[23.] *Kohlhage*, **Über den Zusammenhang zwischen ISA - Toleränz und Oberflächengüte in der Spanenden Fertigungen**, Werkstattstechnik, 55, 1965, 281

[24.] *Karahaliou, H., Petropoulos, G., Petropoulos, P.*, **A Comparative Experimental Study of the Roughness of Metallic Surfaces Machined by Face and Longitudinal Turning**, to be submitted in Wear

UDK 621.91:620.178.16

R. RAKIĆ

The Choice of Lubricating Oil For Rolling Bearings of Machine Tools

RESEARCH

The correct choice of lubricating oil for rolling bearings is essential. The rolling bearings have poor conformity between surfaces, very small contact areas and very high unit loading. The aim of the study presented here is to investigate the influence of lubricating oil on the tribological behaviour of rolling bearings.

To achieve optimum possibility for investigation of tribological properties of lubricating oil for rolling bearings, the author has presented:

- *the classification of industrial oils for rolling bearings of machine tools,*
- *the flowchart of industrial oil selection procedure for rolling bearings in function of all relevant influential factors.*

The experimental investigation of influence of lubricating oils on rolling bearings has been carried out at one metalworking factory.

Key words: lubricating oil, rolling bearings, choice

1. INTRODUCTION

The primary function of the lubricating oil is to separate contacting surfaces, thus preventing metal to metal contact and premature rolling bearing failure. In rolling element bearing operation, elastohydrodynamic lubrication films are generated which reduce the interaction of the contacting surfaces. For rolling bearings, numerous methods have been developed to calculate the thickness of these films, including those by Dowson and Higginson [1], Hamrock and Dowson [2], Hamrock [3] and so on. The differences in the formula apply primarly to different contact geometry.

2. ROLLING BEARINGS

Rolling bearings, as the name indicates, are those in which rolling is the primary form of motion. The majority of bearings used in machines are fitted with rolling bearings. Many factors affect the performance of rolling bearings of machines. Lubrication effects are among the most studied and unfortunately one of the least understood of these factors. One of the attractions of rolling bearings is that they can be operated with little or no clearance, but lubrication is especially important with these and with preloaded bearings, since friction and heat generation are correspondingly increased.

Rolling bearings come in two main varieties on machine tools: ball bearings and roller bearings. As it is shown in Figure 1, this tribomechanical system consists of three elements: element 1 (ball or roller), element 2 (outer and inner ring) and element 3 (lubricant) in which the contact between the two former elements is realised.

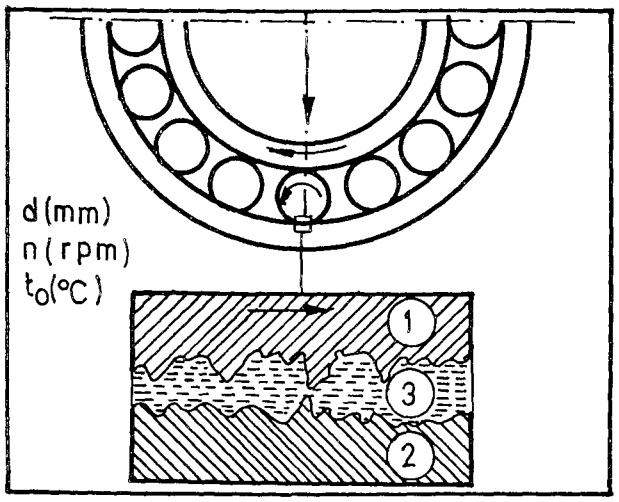

Figure 1. Schematic illustration of rolling bearing

The tribological behaviour of rolling bearings is influenced by a number of factors which are interrelated in complicated ways. The main factors are those varying within allowed ranges in service, i.e. operating temperature (t_o), rotation speed (n), bearing bore (d), lubrication method, etc.

Dr Radoslav Rakić, NIS, Naftagas promet, Novi Sad

3. LUBRICATING OILS

The primary function of a lubricating oil is to separate contacting surfaces, thus preventing metal to metal contact and premature element failure. The lubricating oil must also enable heat removal, protect the highly finished metal surfaces from rusting and other forms of corrosive attack, carry away wear debris and other contaminants.There are two main kinds of lubricants used for lubricated rolling bearings of machines: lubricating oils and greases. When rolling bearings and other tribomechanical systems are incorporated in oil lubricated units, it is both convenient and customary to lubricate them with the same oil used in the machines. The kinds of industrial oils with standpoint ISO recommendation for the choice of lubricants for machine tools [4] and author's investigations [5, 6, 7] are presented in Table 1.

In the column headed "category symbol ISO-L" in Table 1, the various products are designed in an abbreviated form. The prefix letter L designates the class "lubricants, industrial oils and related products". The group of letters which follows the letter L, considered as a whole, forms a code. The first letter of this code identifies the family of the product considered, but the second letter, when it exists, and any following letters, have no particular significance. The numerical group designation which appears after each code corresponds to average kinematic viscosity of the lubricant measured at *40°C* and expressed in millimeters squared per second, i.e. viscosity grades according to ISO 3448.

Table. 1. Classification of lubricating oils for rolling bearings

Letter symbol	Category symbol ISO-L
C	CKB 32 - CKB 68
F	FD 10 - FD 22
H	HM 32 - HM 68
H	HG 32 - HG 68

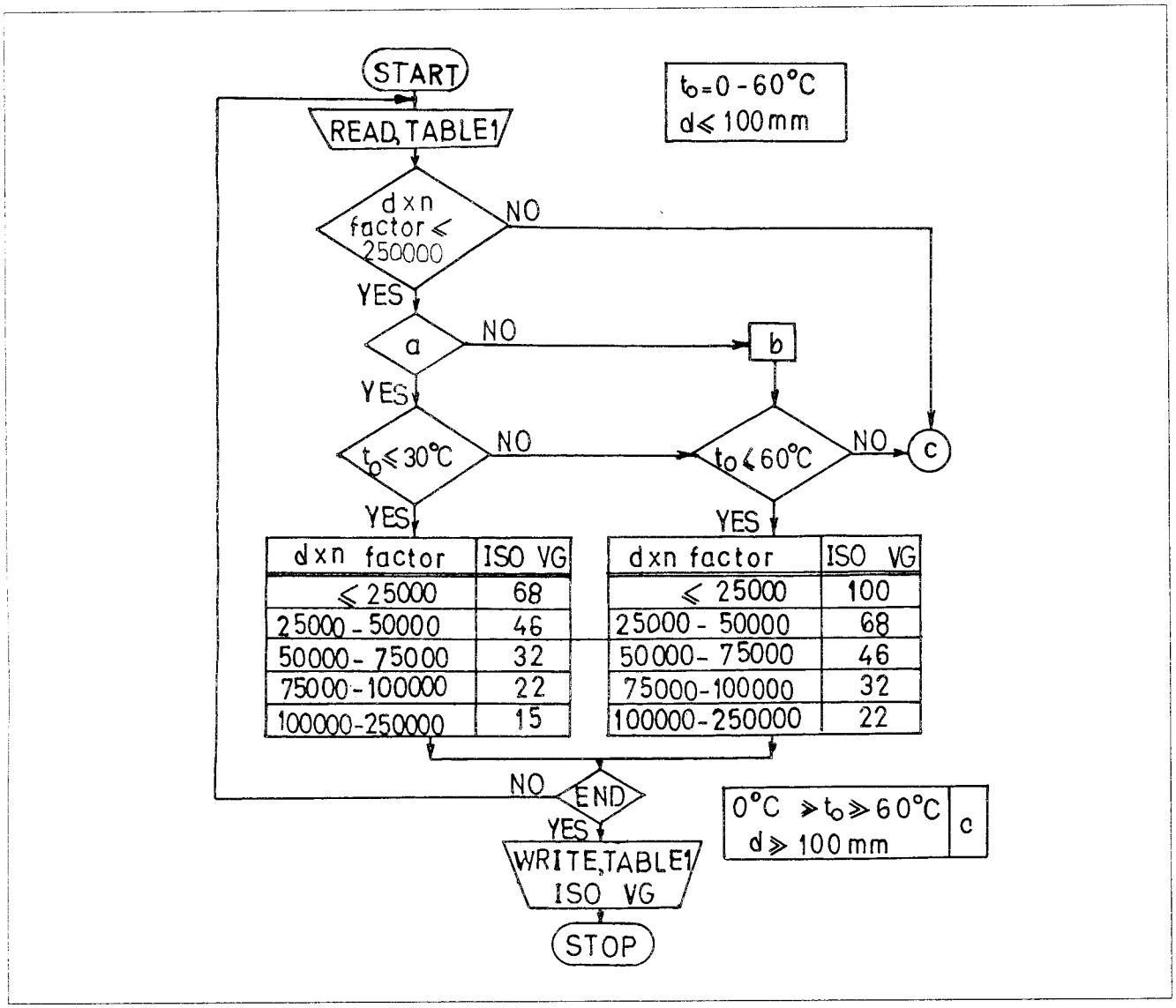

Figure 2. : Flowchart of lubricating oil selection procedure, a- circulating system, b- total loss system, c- go to the other model of decision making

4. SELECTION PROCEDURE OF LUBRICATING OIL

Among many requirements that must be satisfied is optimum lubricant viscosity. To achieve optimum possibility for investigation of the effects of tribological properties of lubricants on tribological behaviour of machine tool rolling bearings, the author has presented the flowchart for determining of the ISO VG characteristic of industrial oils, i.e. ISO Viscosity Grades for rolling bearings. The description of the lubricant selection procedure is given in the form of the flowchart in Figure 2, in function of all relevant influential factors. For this selection procedure, two essential parameters have been taken into account:

- the environment (operating temperature - t_o),
- the rolling bearing operating conditions (rotational speed - n, bearing bore - d, lubrication method).

As it is shown in Figure 2, the selection of the viscosity grade is based on the relationship between the operating temperature and a speed factor (bearing bore (mm) x speed (rpm), normally referred as d x n factor. Greater accuracy can be obtained, for rolling bearing above about *100 mm* bore, by replacing the diameter "*d*" by the arithmetic mean of the outer diameter and bore diameter in mm, sometimes reffered to as the pitch diameter.

5. RESULTS OF EXPERIMENTAL INVESTIGATION

The problems appearing at all rolling bearings very often represent the consequences of tribological processes development on their contact surfaces. The tribological processes on contact surfaces of rolling bearings have been studied by Rakić [5, 6, 7, 8] in function of all influential factors.

The experimental investigation of tribological aspects of lubricating oil choice for rolling bearings have been carried out at one metalworking factory on *120* machine tools (ΣM) in three periods of time, each being *10.000* working hours.

The results of the experimental investigation are presented for three viscosity grades and three types of lubricating oils:

- hydraulic oils, category symbol HM, ISO VG 32 - 68 (I period of time),
- hydraulic oils, category symbol HG, ISO VG 32 - 68 (II period of time),
- gear oils, category symbol CKB (C), ISO VG 32 - 68 (III period of time).

Typical physical properties of these oils are listed in Table 3, 4, and 5, where are : **B** - viscosity at *40°C, mm²/s*; **C** - viscosity index, *min.*; **D** - Flash point, *°C, min*:; **E**- pour point, *°C. max.*

Hydraulic HM oils are based on high refined oils which incorporate additives to enhance: anti-wear performance, oxidation resistance, corrosion protection, pour point, air release and anti-foam properties. Typical physical properties of these oils are listed in Table 2.

Table 2. Hydraulic oils category symbol HM

ISO VG	B	C	D	E
32	32	95	220	-25
46	46	95	220	-25
68	68	95	220	-20

Hydraulic HG oils are based on high viscosity indexed hydrocracked oils which contain selected anti-wear, anti-oxidation and anti-corrosion additives as well as specially developed additives. Typical physical properties of these oils are listed in Table 3.

Table 3. Hydraulic oils category symbol HG

ISO VG	B	C	D	E
32	32	120	220	-25
46	46	120	230	-25
68	98	120	235	-23

Gear CKB (C) oils are based on high refined base oils and contain a specially selected EP additive. Additional additives enhance the anti-corrosion, anti-oxidation, anti-foam properties. Typical physical properties these oils are listed in Table 4.

Table. 4. Gear oils category symbol CKB (C)

ISO VG	B	C	D	E
32	32	95	180	-25
46	46	95	200	-25
68	68	95	210	-25

The rolling bearings operating conditions were:

- the bearing bore $d \leq 100$ *mm*
- $d\,x\,n$ factor ≤ 250000
- the operating temperature $0°C \leq t_o \leq 60°C$

The life time of the rolling bearings up to the failure mostly shows large deviation. By the aid of a probability and statistic methods, it was possible to determine the influence of lubricating oils on the reliability of rolling bearings. The results for three periods of time were plotted in the reliability curves versus time shown in Figures: 3, 4 and 5.

Figure 3 shows the curves of rolling bearings reliability "R" versus time "T" as a function of the ISO VG of hydraulic oil ISO-L-HM.

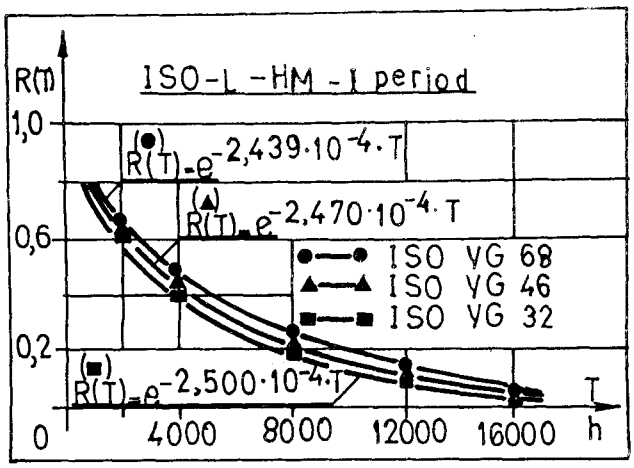

Fig. 3. Reliability of rolling bearings versus time for ISO-L-HM

Figure 4 shows the curves of rolling bearings reliability "R" versus time "T" as a function of the ISO VG of hydraulic oil ISO-L-HG.

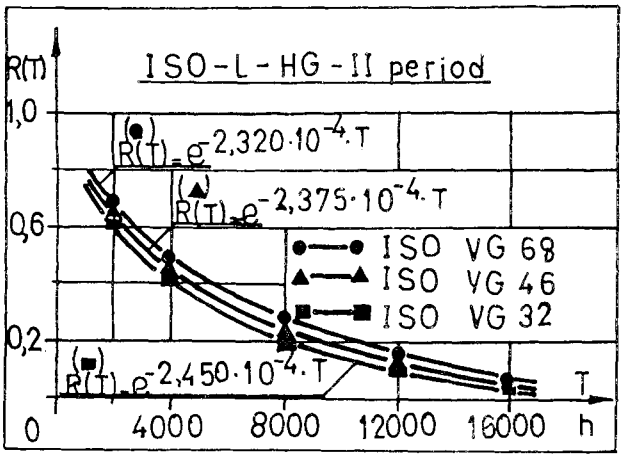

Fig. 4. Reliability of rolling bearings versus time for ISO-L-HG

Figure 5 shows the curves of rolling bearings reliability "R" versus time "T" as a function of the ISO VG of gear oil ISO-L-CKB (C).

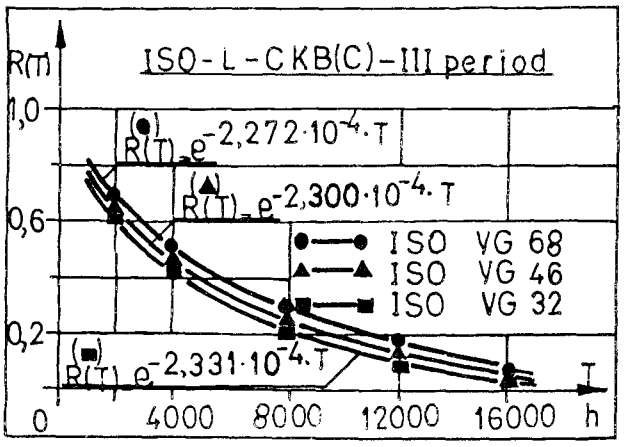

Fig. 5. Reliability of rolling bearings versus time for ISO-L-CKB (C)

6. CONCLUSION

The following conclusions can be drawn from the results presented above:

- the reliability of rolling bearings were found to be affected by both viscosity grade and type of lubricating oil.
- the hydraulic oil ISO-L-HG gives a longer rolling bearings life compared with the case the hydraulic oil ISO-L- HM.

the gear oil ISO-VG 68 gives the longest rolling bearings life among all the lubricating oils studied in the present work, under presented operating conditions of investigation.

The obtained results proved that the tribological properties of lubricating oils have quite great influence on the rolling bearings. The right choice of the lubricating oil may be prolonged the life of rolling bearings of machines, better utilised of lubricating oil and decreased of lubricating oils consumption.

REFERENCES

[1.] *Dowson D., Higginson G. R.*, **Elastohydro-dynamic Lubrication**, Pergamon Press, Oxford, 1966.

[2.] *Hamrock B. J., Dowson D.*, **Ball Bearing Lubrication of Elliptical Contacts**, John Willey, Interscience Publishers, New York, 1980.

[3.] *Hamrock B. J.*, **Elastohydrodynamic Lubrication of Elliptical Contacts**, Proceedings of the 1st Symposium "Intertribo 81", High Tatras, Czechoslovakia, 1981, 6-16.

[4.] ISO Technical Report 3498, **Lubricants, Industrial oils and related products (class L)-Recommendation for the choice of lubricants for machine tools**, 1986.

[5.] *Rakić R.*, **Tribological Properties of Lubricants on Machine Tool Rolling Bearings as Factor of their Reliability**, Proceedings of the 3rd International Symposium of Tribology, High Tatras, Czechoslovakia, 1987, 384-389.

[6.] *Rakić R.*, **Reliability and Tribological Properties of Lubricants on Machine Elements in Nonconformal Contact**, proceedings of the IX Nat. Conference on Industrial Tribology, Bangalore, India, 1991, L.167-175.

[7.] *Rakić R.*, **The Influence of Tribological Properties of Lubricants on the Tribomechanical System Elements on Nonconformal Contact**, Proceedings of the 6th International Congress on Tribology, Budapest, Hungary, 1993, Vol. 2., 228-233.

[8.] *Rakić R.*, **The Effects of Tribological Processes on Reliability of Rolling Bearings**, Proceedings of the 13th Int. Conference on Production Research, Jerusalem, Israel, 1995, 274-276.

UDK 621.91:620.178.16

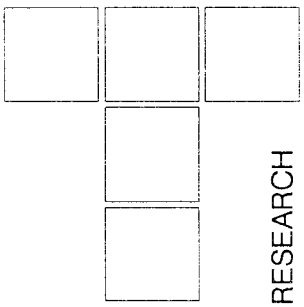

DUMITRU AMARANDEI, EUGEN CEFRANOV,
LUCION SEVERIN, DAN SEMENCIUC

Experimental Research Concerninig The Value of The Average Friction Coefficient on The Rake Tool Surface in Carbon Steel Turning

This paper shows a physical-mathematical model for calculating the average friction coefficient, applicable in high speed cutting with single tooth tool, where both the physical scomponents of the cutting force (Fx, Fy, Fz) and the geometry of the tool (the rake angle and the tool's edge incilination angle κ) are taken into account. There are also shown experimental results and conclusions regarding the influence of the cutting parameters, the work material, the tool's material and the cutting conditions for speeds up to 1000 m/min.

Keywords: *average friction coefficient, rake angle, cutting force, turning*

1. INTRODUCTION

The development and the normal evolution of the machining proceedings, starting with cutting speeds of tenths of meters/minute in 1800, to 100 m/min in 1996, definitely imposed a continuos tendency of studying these processes, taking into account the elements which contribute to their evolution, the working conditions and the machining parameters.

The necessity ameliorating the technical-economical conditions for the development of the cutting process, along with the higher demands of the world aeronautics in the last years (which is very much dependent on the materials with special mechanical properties and special metallic alous), have imposed as a machining method "the high speed machining". At high speeds, because the phenomena accompanying the process are modified and less explained, new models and new relations, allowing to understand the specific mechanisms of the high speed cutting and their dependecne on speed and on other basic parameters of the cutting process, were imposed.

This paper refers to a calculating model used by the authors in experimental research of the average friction coefficient on the rake surface in high speed turning of the OLC 45 carbon steel.

Reader Dr. Eng. Dumitru AMARANDEI,
Professor Dr. Eng. Eugen CEFRANOV,
Reader Dr. Eng. Lucion SEVERIN,
Lecturer Eng. Dan SEMENCIUC,
"Stefan cel Mare" University of Suceava, Romania

2. THEORETICAL CONSIDERATIONS

The informations relative to the cutting process mechanics, contained in recent literature, allowed to conclude that Merchant and Ernst's model remains justified only for orthogonal cutting, below a certain "critical speed" [5, 7, 8, 12, 17, 18, 19]. For higher speeds, the conventional force's circle from the Merchant's model must be completed with other components, as the inertial force [1, 3].

During the cutting process, the tool acts above the detached layer and the machined piece, the tool supporting itself the pressure due to the normal coponent F_N and the friction force F from the rake surface, and the machined surface supporting the pressure due to the normal component F' and the friction force F'_N from the flank surface, figure 1, [4].

The information referring to all these forces and to the friction phenomena in cutting are important not only in theory, but also in practice, their value influencing the cutting forces in the conditions that make the cutting possible [13].

In many papers the friction on the flank surface of the tool is much smaller (μ_a=*0.1...0.7*) than the friction on the rake surface (μ_γ=*0.1...0.7*) and it is negligible; the friction on the interface chip-tool being more important,

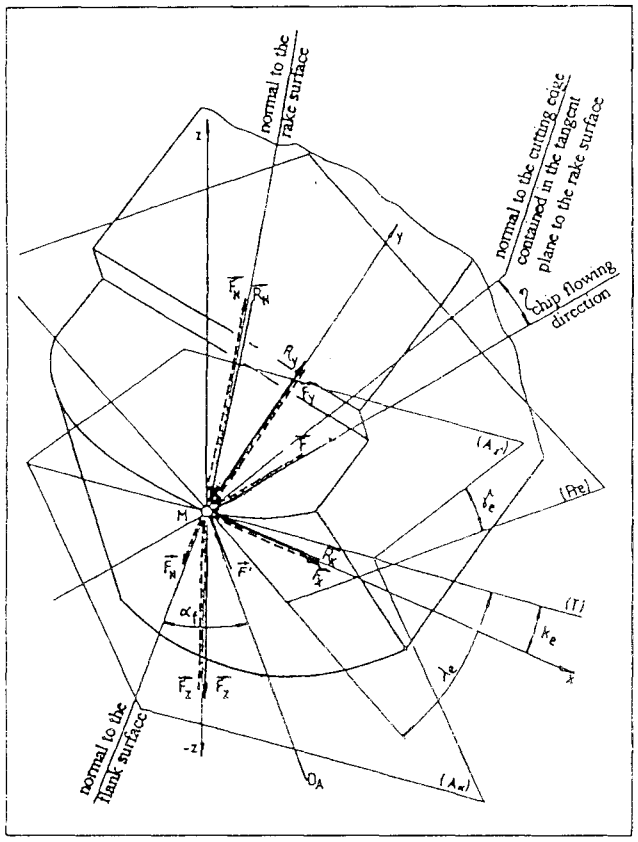

Figure 1. Phisical-geometrical model for cutting

because in reality it represents the greater percentage in total amount of the cutting force [15].

In these conditions, the relations provided by the literature of speciality [3] for calculating the average coefficient of friction in normal cutting speeds, must be revised and completed to be also available for greater speeds. Below is presented such a mathematical model for calculating the average coefficient of friction, that is an extension of Merchant's model established for semi-orthogonal turning and applicable in HSM.

3. PSYSICAL AND MATHEMATICAL MODEL FOR CALCULATING THE AVERAGE FRICTION COEFFICIENT

The establishment of the mathematical model for the average coefficient of friction $\mu_{\gamma M}$ was made based on the known relations (1) of the cutting theory for a cutting tooth (figure 2), as function of the plastic deformation force F_N, the external angle of friction ρ, the rake angle in the normal plane to the tool's edge γ_{N0}, the edge's inclination angle λ and the edge cutting angle κ.

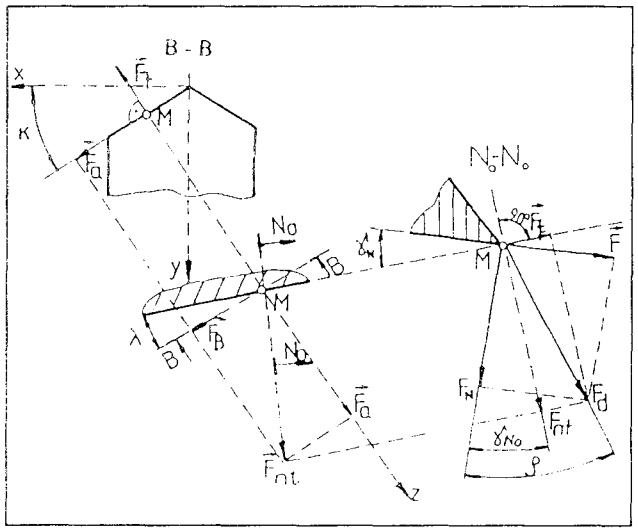

Figure 2. Calculating model for the components F_x, F_y, F_z as function of F_N and F [3]

$$F_x = +\frac{F_N}{\cos\rho}\cdot\cos(\rho-\gamma_{No})\cdot\sin\lambda\cdot\cos\kappa+\frac{F_N}{\cos\rho}\cdot\sin(\rho-\gamma_{No})\cdot\sin\kappa$$

$$F_y = -\frac{F_N}{\cos\rho}\cdot\cos(\rho-\gamma_{No})\cdot\sin\lambda\cdot\sin\kappa+\frac{F_N}{\cos\rho}\cdot\sin(\rho-\gamma_{No})\cdot\cos\kappa \qquad (1)$$

$$F_z = +\frac{F_N}{\cos\rho}\cdot\cos(\rho-\gamma_{No})\cdot\cos\lambda$$

$$\cos(\rho-\gamma_{No}) = \cos\rho\cdot\cos\gamma_{No}+\sin\rho\cdot\sin\gamma_{No}$$

$$\sin(\rho-\gamma_{No}) = \sin\rho\cdot\cos\gamma_{No}-\cos\rho\cdot\sin\gamma_{No} \qquad (2)$$

Using the fundamental relations (2) for the components F_x, F_y, F_z, the relations (3) result as

$$F_x = +F_N\cdot(\cos\gamma_{No}+\mu_{\gamma M}\cdot\sin\gamma_{No})\cdot\sin\lambda\cdot\cos\kappa+F_N\cdot(\mu_{\gamma M}\cdot\cos\gamma_{No}-\sin\gamma_{No})\cdot\sin\kappa$$

$$F_y = -F_N\cdot(\cos\gamma_{No}+\mu_{\gamma M}\cdot\sin\gamma_{No})\cdot\sin\lambda\cdot\sin\kappa+F_N\cdot(\mu_{\gamma M}\cdot\cos\gamma_{No}-\sin\gamma_{No})\cdot\cos\kappa \qquad (3)$$

$$F_z = +F_N\cdot(\cos\gamma_{No}+\mu_{\gamma M}\cdot\sin\gamma_{No})\cdot\cos\lambda$$

If we substitute F_N in the first two relations (3) with the relation (4), obtained from the third relation (3) then for the components F_x, F_y we have:

$$F_N = \frac{F_z}{(\cos\gamma_{No} + \mu_{\gamma M} \cdot \sin\gamma_{No}) \cdot \cos\lambda} \tag{4}$$

$$\begin{aligned} F_x &= +F_z \cdot tg\lambda \cdot \cos\kappa + F_z \cdot \frac{\mu_{\gamma M} \cdot \cos\gamma_{No} - \sin\gamma_{No}}{\cos\gamma_{No} + \mu_{\gamma M} \cdot \sin\gamma_{No}} \cdot \frac{\sin\kappa}{\cos\lambda} \\ F_y &= -F_z \cdot tg\lambda \cdot \sin\kappa + F_z \cdot \frac{\mu_{\gamma M} \cdot \cos\gamma_{No} - \sin\gamma_{No}}{\cos\gamma_{No} + \mu_{\gamma M} \cdot \sin\gamma_{No}} \cdot \frac{\cos\kappa}{\cos\lambda} \end{aligned} \tag{5}$$

Developing the ratios F_x/F_z, F_y/F_z as relations (6) and using the notations (7) we can obtain the relation (8). By similar procedure for $\mu_{\gamma M}$ the relation (9) is obtained.

$$\begin{aligned} \frac{F_x}{F_z} &= +tg\lambda \cdot \cos\kappa + \frac{\mu_{\gamma M} \cdot \cos\gamma_{No} - \sin\gamma_{No}}{\cos\gamma_{No} + \mu_{\gamma M} \cdot \sin\gamma_{No}} \cdot \frac{\sin\kappa}{\cos\lambda} \\ \frac{F_y}{F_z} &= -tg\lambda \cdot \sin\kappa + \frac{\mu_{\gamma M} \cdot \cos\gamma_{No} - \sin\gamma_{No}}{\cos\gamma_{No} + \mu_{\gamma M} \cdot \sin\gamma_{No}} \cdot \frac{\cos\kappa}{\cos\lambda} \end{aligned} \tag{6}$$

$$\begin{aligned} A &= +tg\lambda \\ B &= + \frac{\mu_{\gamma M} \cdot \cos\gamma_{No} - \sin\gamma_{No}}{\cos\gamma_{No} + \mu_{\gamma M} \cdot \sin\gamma_{No}} \cdot \frac{1}{\cos\lambda} \end{aligned} \tag{7}$$

$$\begin{aligned} \frac{F_x}{F_z} &= +A \cdot \cos\kappa + B \cdot \sin\kappa \\ \frac{F_y}{F_z} &= -A \cdot \sin\kappa + B \cdot \cos\kappa \end{aligned} \tag{8}$$

$$\mu_{\gamma M} = \frac{\sqrt{\left[\left(\frac{F_x}{F_z}\right)^2 + \left(\frac{F_x}{F_z}\right)^2\right] \cdot \cos^2\gamma - \sin^2\lambda} + tg\gamma_{No}}{1 - tg\gamma_{No} \cdot \sqrt{\left[\left(\frac{F_x}{F_z}\right)^2 + \left[\left(\frac{F_x}{F_z}\right)^2\right] \cdot \cos^2\gamma - \sin^2\lambda}} \tag{9}$$

The relation (9) describes the connection between the average friction coefficient and the components F_x, F_y and F_z of the cutting force, the rake angle, γ_{No}, and the edge's inclination angle, λ.

As a result, obtaining the values for that coefficient resumes in these conditions to experimental determination of the components of the cutting force and measuring the tool's angles. Some separate cases can be distinguished:

a) for null edge's inclination angles ($\lambda=0^o$), the angle γ_{No} becomes γ_N ($\gamma_{No}=\gamma_N\neq 0^o$), and the relation (9) takes the form (10), which in coordinates (F_x/F_z, F_y/F_z) represents the equation of a circle with radius r, relation (1), figure 3.

b) for $\lambda=0^o$ and $\lambda_{No}=\lambda_N=0^o$ the relation (10) takes the form of the expression (12), which is the equation of a circle with radius $r=\mu_M$ *(figure 3)*.

$$\mu_{\gamma M} = \frac{\sqrt{\left[\left(\frac{F_x}{F_z}\right)^2 + \left(\frac{F_x}{F_z}\right)^2\right]} + tg\gamma_N}{1 - tg\gamma_N \cdot \sqrt{\left[\left(\frac{F_x}{F_z}\right)^2 + \left[\left(\frac{F_x}{F_z}\right)^2\right]}} \tag{10}$$

$$r = \frac{\mu_{\gamma M} - tg\gamma_N}{1 + \mu_{\gamma M} \cdot tg\gamma_N} \tag{11}$$

$$\mu_{\gamma M} = \sqrt{\left[\left(\frac{F_x}{F_z}\right)^2 + \left(\frac{F_x}{F_z}\right)^2\right]} \tag{12}$$

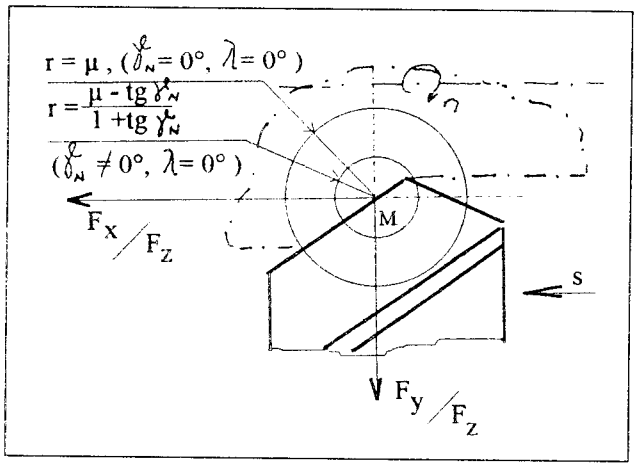

Figure 3. Curves for the average friction coefficient in coordinates (F_x/F_z, F_y/F_z)

c) for $\lambda=0^o$, $\gamma_{No}=\gamma_N\neq 0^o$ and $F_{ox}=0$, as for the transversal turning, relation (9) takes the form of Merchant's relation for the orthogonal turning (13).

$$\mu_{\gamma M} = \frac{\frac{F_x}{F_z} + tg\gamma_N}{1 - tg\gamma_N \cdot \frac{F_y}{F_z}} = \frac{F_y + F_z \cdot tg\gamma_N}{F_z - F_y \cdot tg\gamma_N} \tag{13}$$

All these allow us to say that the relation (9), proposed for calculating the "average friction coefficient", is in fact an extension of Merchant's relation from the orthogonal cutting case to oblique cutting case.

4. EXPERIMENTAL REULTS AND ANALYSIS.

4.1. Machining conditions.

Experiments were conducted on a modified lathe, with a *16 Kw* engine and an electronic rotation variator. The piece was a disk one, mounted between chuck and dead centre, from OLC 45 steel. The tool was a mineral-ceramic SiAlON CC 680E, SNUN type, with the following angles: $\kappa=70^o$, $\gamma_{No}=6^o$, $\alpha=6^o$. Measurement of the forces was done using a piezo-electrical triple-axial dynamometer type 9257A (Kistler) in a measurement chain that

also included an amplifier, a recording apparatus and a PC computer. Experimental values for the components F_x, F_y and F_z were found, and they allowed to calculate the average friction coefficient with the relation (9).

The variation curves of the friction coefficient on the rake surface as function of the machining parameters and tool geometry, obtained in OLC 45 machining are shown in figures 5 to 10.

In order to establish the variation law of the friction coefficient ($\mu_{\gamma M}$) an experimental optimised plan was realised from 32 experiments (table 2), taken from the table $L_{32}(2^{31})$ after Tagouchi method [13], for the mathematical model given by the relation (14), which has the graph from the figure 4.

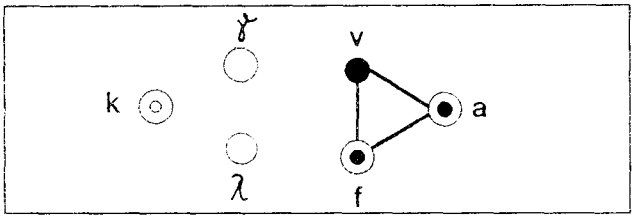

Figure 4. Linear graph of model 14

The values (levels) taken by the cutting process parameters during the experiments were those shown in table 1. Table 2 and the relations (15) present the result of the experiments done according to plan, respectively, the approximating functions for the effects and the interactions between the factors, and the variation law of the friction coefficient ($\mu_{\gamma M}$) on the rake surface.

$$\mathbf{Y \approx M + v + s + t + k + \gamma + \lambda + vxs + vxt + sxt + vxsxt\ ;}$$

Levels		4	4	2	2	2	2	4x4	4x2	4x2		
Degres of freedom	1	3	3	1	1	1	1	9	3	3	1	$\Sigma = 26$

(14)

$$\mu_{\gamma M} = M + [v^3 v^2 v1]\,x\,Av + [s^3 s^2 s1]\,x\,As + [ln(t)\ 1]\,x\,At + [ln(k)\ 1]\,x\,Ak + [ln(\gamma)\ 1]\,x\,A\gamma +$$

$$+ [ln(\lambda)\ 1]\,x\,A\lambda + [v^3 v^2 v1]\,x\,Avs\,x\begin{bmatrix} s^3 \\ s^2 \\ s \\ t \end{bmatrix} + [v^3 v^2 v1]\,x\,Avt\,x\begin{bmatrix} t \\ 1 \end{bmatrix} + [s^3 s^2 s1]\,x\,Ast\,x\begin{bmatrix} t \\ 1 \end{bmatrix} \quad (15)$$

The Snedecor test (table 3) shows that speed has a singificant influence on the coefficient, and feed and the cutting depth, by the area of the contact surface, the value of plastic deformations and the interactions among $v\,x\,s$, $v\,x\,t$ and $s\,x\,t$. The edge cutting angle, the rake and the flank angle, the edge's inclination angle have insignificant influence, the most important one being that of the edge's inclination angle.

4.2. Result's analysis

The intensifying of the cutting parameters generates temperatures, which in the sharing plane are high enough to diminish the mechanical properties of the work material, so causing that some already known conclusions about the cutting process become not conclusive. The present research allowed to formulate some conclusions about the experimental values of the average friction coefficient and the influence of the main cutting conditions on it.

For speeds of *100...250 m/min*, the cutting temperature rises, influencing the mechanical characteristics of the working steel. So, the flowing resistance of the material is increasing a little. For speeds greater than *250 m/min*, the temperature reaches *1000°C*, the material becomes plastified much stronger and the flowing resistance decrease.

The variation curves from figure 5 show that the values of the friction coefficient ($\mu_{\gamma M}$) on the rake surface de-

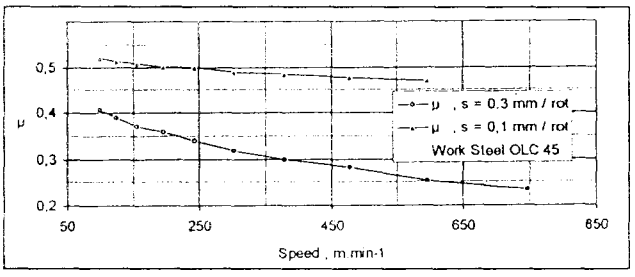

Figure 5. Influence of the cutting speed on the friction coefficient $\mu_{\gamma M}$

Table 1. Values of the studied factors

Factors	n [rot/min]	v [m/min]	s [mm/min]	a [mm]	κ [°]	γ [°]	λ [°]
Values	246	100.4	0.1	1.0	45	-6	-6
	747	302.5	0.2	1.5	90	0	0
	1470	595.4	0.3				
	1844	746.9	0.5				

Table 2. Experimental Tagouchi plan for theoretical-experimental determin of the friction coefficient ($\mu\gamma_M$)

Nr. experim.	v	s	t	k	λ	γ	Calculated values for the average coefficient		r	r^{2} x 10-3
							$\mu\gamma_M$	$\approx\mu\gamma_M$	$(\mu\alpha - \mu\alpha_T)$	$(\mu\alpha - \mu\alpha_T)^2$
1	1	1	1	1	1	1	0.620	0.616	+0.004	0.016
2	4	3	1	1	1	1	0.313	0.337	-0.024	0.576
3	1	2	2	1	1	1	0.324	0.351	-0.027	0.729
4	4	4	2	1	1	1	0.119	0.070	+0.049	2.401
5	3	3	2	2	1	1	0.210	0.234	-0.024	0.576
6	2	1	2	2	1	1	0.360	0.346	+0.020	0.400
7	3	4	1	2	1	1	0.179	0.146	+0.033	1.089
8	2	2	1	2	1	1	0.297	0.318	-0.027	0.729
9	3	1	2	1	2	1	0.533	0.485	+0.048	2.304
10	2	3	2	1	2	1	0.389	0.432	-0.043	1.8049
11	3	2	1	1	2	1	0.483	0.492	-0.009	0.081
12	2	4	1	1	2	1	0.273	0.269	+0.004	0.016
13	1	3	1	2	2	1	0.437	0.480	-0.043	1.849
14	4	1	1	2	2	1	0.351	0.258	+0.064	4.096
15	1	4	2	2	2	1	0.256	0.267	-0.011	0.121
16	4	2	2	2	2	1	0.311	0.320	-0.009	0.081
17	1	3	2	1	1	2	0.310	0.267	+0.043	1.849
18	4	1	2	1	1	2	0.214	0.277	-0.063	3.969
19	1	4	1	1	1	2	0.320	0.309	+0.011	0.121
20	4	2	1	1	1	2	0.273	0.264	+0.009	0.081
21	3	1	1	2	1	2	0.359	0.407	-0.048	0.304
22	2	3	1	2	1	2	0.301	0.258	+0.043	1.849
23	3	2	2	2	1	2	0.231	0.222	+0.009	0.081
24	2	4	2	2	1	2	0.196	0.200	-0.004	0.0160
25	3	3	1	1	2	2	0.460	0.436	+0.024	0.576
26	2	1	1	1	2	2	0.345	0.364	-0.019	0.361
27	3		2	1	2	2	0.140	0.172	-0.032	1.024
28	2	2	2	1	2	2	0.451	0.424	+0.027	0.729
29	1	1	2	2	2	2	0.700	0.704	-0.004	0.016
30	4	3	2	2	2	2	0.565	0.540	+0.025	0.625
31	1	2	1	2	2	2	0.740	0.712	+0.028	0.784
32	4	4	1	2	2	2	0.162	0.210	-0.048	2.304
							11.2224	-	0	29.298
							0.3507		-	-

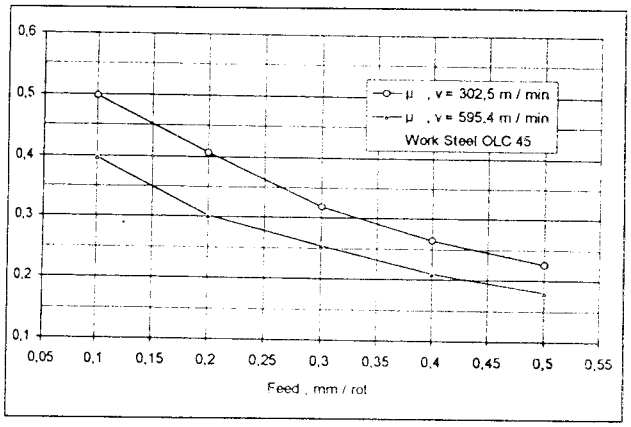

Figure 6. Influence of the feed on the friction coefficient $\mu_{\gamma M}$

crease with an average of *42%* (more strongly normal speeds), when speed increases up to *1000 m/min.*

The significant influence of the feed on the friction coefficient, in oblique turning of the OLC 45 steel is shown in figure 6. It results that between *250 m/min* and 1000 m/min the coefficient goes down from *0.5 to 0.2*. The decreasing tendency of the friction coefficient while the feed increases, can be explained by the much slower increase of the tangential friction stresses (τ) on the contact surface, as reported for the normal stress (σ) due to the intensifying of the thermic effect.

The increasing of the cutting depth in oblique turning of the steel (figure 7) is accompanied by an increase of the

Table 3. Snedecor test for analizing the dispersion of the factors influencing the friction coefficient

Factors	Sum $S_i \times 10^{-3}$	degrees of freedom n_i-1	Variance $V_i=S/(n_i-1)\times10^{-3}$	$F_{\mu_{\gamma M}}=\frac{V_i}{V_R}$	$F_{SNEDECOR}$ p = 0.95%	Significant YES ($F_{\mu_{\gamma M}}>F_S$) NO ($F_{\mu_{\gamma M}}<F_S$)
v	142.58	3	47.586	9.745	4.76	YES
s	242.23	3	80.742	16.471	4.76	YES
t	30.9	1	30.95	6.38	5.99	NO
K	0.25	1	0.250	0.051	5.99	NO
g	0.12	1	0.122	0.024	5.99	NO
l	3.07	1	3.073	0.626	5.99	NO
v x s	121.43	9	13.493	2.752	4.10	NO
v x t	48.48	3	16.163	3.297	4.76	NO
s x t	25.49	3	8.499	1.733	4.76	NO
Rest	29.29	6	4.883			
Total	624.11	31				

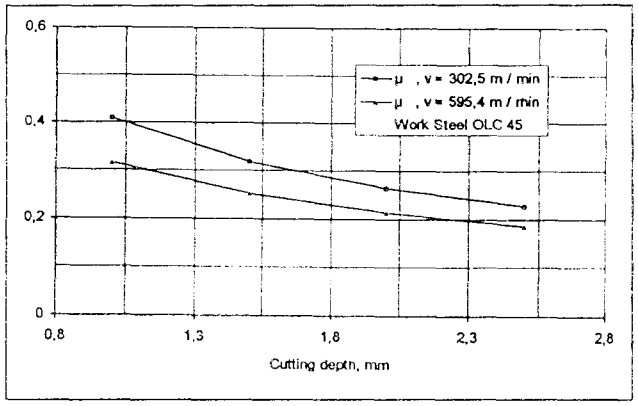

Figure 7. Influence of the cutting depth on the friction coefficient $\mu_{\gamma M}$

values for the cutting force's components, but also the thermic effect is intensifying. That determines a decrease of the specific pressure on the contact surfaces and of the values of the friction coefficient.

The increasing of the values for the cutting edge angle from *45° to 90°* determines the increase of the thickness and the decrease of the breadth of the chip, and thus the specific cutting forces decrease and the specific unit charge rise. The variation curves of figure 8, for the friction coefficient on the rake surface, show that the

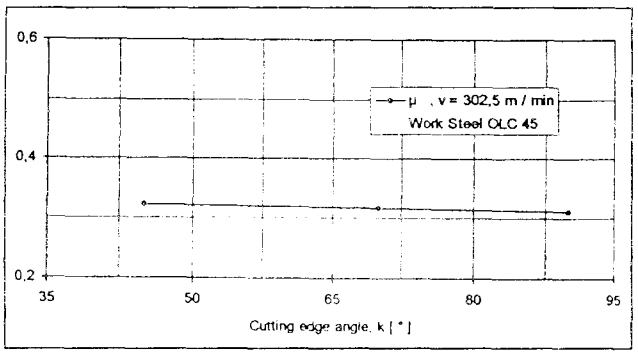

Figure 8. Influence of the cutting edge angle on the friction coefficient $\mu_{\gamma M}$

intensity of the friction decreases with an average of *2.5%* and the specific pressure with *0.4%*. According to Snedecor test it results that the influence of that angle on the average friction coefficient is insignificant as reported to the cutting parameters influence.

The curves in figure 9 show the direct influence of the rake angle on the average coefficient. For a speed of *302.5 m/min* and a chip's cross section of *0.3x1.5 mm²* the friction coefficient increases for greater values of the rake angle. At the same time the plastic deformation forces decrease, and also the specific pressure on the rake surface, under the assumption that the friction

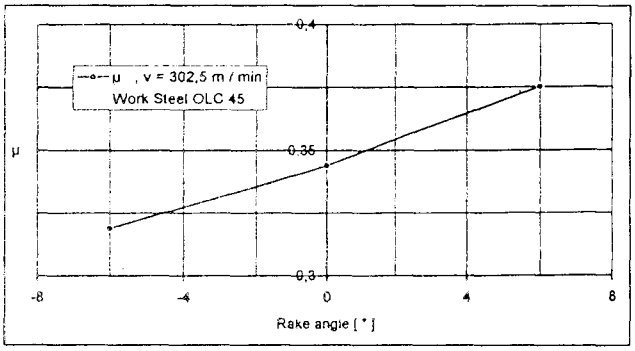

Figure 9. Influence of the rake angle on the friction coefficient $\mu_{\gamma M}$

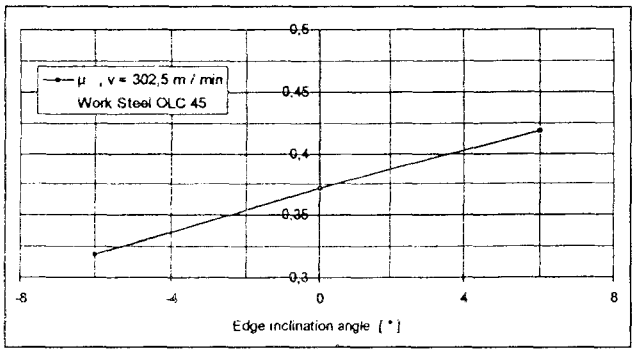

Figure 10. Influence of the edge inclination angle on the friction coefficient $\mu_{\gamma M}$

stress is contant on the contact area depending on γ, and the friction coefficient increase according to figure 9. A similar influence, figure 10, has the edge cutting angle κ.

5. CONCLUSIONS

This paper shows a calculus model for the average friction coefficient on the contact surface between tool and chip, under the assumption that the friction on the flank surface is null. The relation obtained is an extension of Merchant's relation and shows that the coefficient depends on the values of the components F_x, F_y and F_z the cutting forces and the geometry of the tool through the edge's inclination angle (λ) and the rake angle (γ).

The analysis of dependencies from figures 5 to 10 and of the values obtained with relation (9), for the average friction coefficient $\mu_{\gamma M}$ shows that the dependence of the coefficient's values on the machining parameters and the tool geometry is also confirmed by results obtained by other authors [1, 3, 4, 14, 15].

NOTATIONS:

v - *cutting speed;*
f_{xa} - *chip's cross section;*
μ_α - *friction coefficient on the flank surface;*
μ_γ - *friction coefficient on the rake surface;*
$\mu_{\gamma M}$ - *average friction coefficient, rake surface;*
τ, σ - *tangential, normal stresses, rake surface;*
(P) - *base plane;*
$(A\alpha)$ - *tangent plane to the flank surface, in M;*
$(A\gamma)$ - *tangent plane to the rake surface, in M;*
(P_{re}) - *pressure plane (normal to the effective speed vector $\vec{v}_e$ - the resultant speed, at point M);*
$\bar{T}$ - *tangent to the cutting edge, at point M;*
$\kappa, \gamma, \alpha, \lambda$ - *tool angles: tool cutting edge angle, tool rake angle, tool flank angle, tool cutting edge inclination angle respectirely;*
$\kappa_e, \gamma_e, \alpha_e, \lambda_e$ - *working angles: working cutting edge angle, working minor cutting edge angle, working rake angle, working flank angle, working cutting edge inclination angle respectirely;*
η - *angle between the chip's flowing direction and the $\vec{N}$ vector measured in (A_γ) plane;*
γ_N, α_N - *rake angle and flank angle in the secant plane N_0-N_0 respectirely;*
N_0-N_0 - *secant plane;*
Fd - *cutting force;*
F_N - *plastic deformation force;*
F - *friction force;*
F_a - *cutting force's component, normal to the cutting edge, in a plane parallel to the base plane;*
$\bar{F}_t$ - *cutting force's component, along the cutting edge in plane orthogonal to rake surface;*
$\bar{F}_{nt}$ - *cutting force's component, orthogonal to cutting edge in tangent plane with the rake surface.*

BIBLIOGRAPHY

[1.] *Amarendei, D.*, **Methodes experimentales appliquees a la modelisation de l' usinage par outil coupant dans le but de la determination des forces de deformation plastique et de frottement pendant la coupe a grande vitasse**, Memoire du Diplome d' Etudes Approfondies de Mecanique, INSA Lyon, France, 1993.

[2.] *Amarandei, D., Cozminca, M. Mironeasa, C.*, **Relative de calcul a coeficientului de frecare la aschiere, Analele universitatii**, Sectiunea Mecanica, nr. 1-6, Suceava, 1993, p. 50-52.

[3.] *Amarandei, D.*, **Cercetari privind marimea forpelor de deformare plastica si de frecare la aschierea cu vieze mari a opelurilor carbon**, Teza de doctorat, Univ. "Gh. Asachi" Iasi, 1996.

[4.] *Amarandei, D.*, **Experimental method applied for modelling edge tool cutting with aim of evaluation the plastic deformation and friction forces at HSM**, 4-TH Yugoslav Conference of Tribology, 27-29 sept. 1995. Belgrade.

[5.] *Arndt, G.* **Ultra-High-Speed Machining: Review and Analysis of Cutting Forces**, Proc. Inst. Mech. Engrs. 1973, vol.187, 44/73, pag.625-634.

[6.] *Arndt, G.*, **Ultra-High-Speed Machining**, Annals of the CIRP, vol. 21/1, 1972.

[7.] *Elepin, A.P.*, **Scorostnoe rezanie i ego effectihnosti pri obrabotke vleakik materialov**, Sb. Nauki, TR /Gorki, Vod. Transp., 1988, no. 233, pag. 55-62.

[8.] *Erdal, E., Elijah, K., Asibu, JR.*, **Acoustic emission and Force sensor Fusion for monitoring the Cutting Proces**, Int. J. Mech. Vol. 31, No. 11/12, pag. 795 - 809, 1989.

[10.] *Ernst, H., Merchant, M.E.*, **Chip Formation Friction and High Quality Machining, Surface Treatment of Metals**, Prep, 53, ASME, 1941.

[11.] *Ippolito, R., Tornincasa, S., Elepin, E.*, **Matrix Representation and Prediction of 3D Cutting Forces**, Journal of Engineering for Industry Nov. 1977. Pag. 829-835.

[13.] *Korneeva, V., Kamalov, S.*, **Temperatura rezaniea pri obrabotke metallov so sverhvisokimi scorosteami, Izvestia vissih ucebnih zavedenii**, Masinostroenie, nr. 2, 1986, p.142-146.

[14.] *Kravceko, V.A.*, **O vleanii parametrov obrabotki na sili deisvuosie na zadnei povernosti instrumenta**, Vestnik Masinostr., nr. 6, 1989, p.41-43.

[15.] *Kronenberg, M.*, **Machining Science, Application**, London, 1966.

[16.] *Maurice Pilet*, **Introduction aux plans d'experiences par la methode Tahouchi**, Universite de Cachan, 1992, ISBN 2-70811-1442-5, France.

[17.] *Molinari, A., Dudzinski, D.*, **A Dymamic Analysis of High - Speed Machining**, Journal of Engineering for Industry, Nov. 1985, vol. 107, pag. 309-315.

[18.] *Recht R. F.*, **A Dynamic Analysis of High-Speed Machining**, Journal of Engineering for Industry Nov. 1985, vol. 107, pag. 309-315.

[19.] *Zorev, N.*, **Despre interdependenta proceselor din zona formarii aschiei si din zona de contact a fetei de degajare a sculei**, Vestnik Masinostr., 43, nr. 12, 1963, p.42-50.

UDK 621.178.91.003.12

RESEARCH

I. TUDOR, R. RAPEANU

Minimising Wear by Weld Covering with Metallic Carbide Recovered at Grinding

The refuses, as powder, resulted at metallic carbide layers grinding, include many scarce elements, with great hardness like W, Ti, Cr carbides and also Co or Ni as matrix.

We develop a magnetic method to separate metallic powder from abrasive non-metallic powder.

The recovered powder could serve to fill up tubular electrodes destined for weld loading at wear exposed surfaces. We determine tribological characteristics obtained on layers, and the proper support between electrode core and wall, and a number of stratums for maximum hardness.

Keywords: wear, weld loading, grinding, metallic carbide, magnetic hardness, friction coefficient.

1. GENERAL ASPECTS

Hardness growth at surfaces working in condition of adhesion, corrosion, abrasion wear, is possible by weld loading with metallic carbide.

The most utilised coatings are based on rellit and stellit. The refuses, as powder, resulted at metalic carbide layers grinding, include many scarce elements, with great hardness like W, Ti, Cr, carbides that are theoretic diamagnetic.

We develop a magnetic method to separate metallic powder from abrasive non-metallic powder because in weld process exists a dilution between ferrous and W, Ti, Cr carbides.

The recover powder could serve to fill up tubular electrodes destined for weld loading at wear exposed surfaces.

2. METALLIC POWDER SEPARATION

Metalic powders from grinding refuse are magnetically separated in dry way. At coarse grind were used cutting compounds like anhydrous sodium carbonate with $pH=8.5\text{-}9.5$. The refuse is washed in jet of water in reverse circulation till $pH=7\text{-}7.5$. For our testing washing water necessary was *7 litter/1Kg* powder refuses.

Tudor Ioan,
Rapeanu Razvan,
University "Petroleum-Gas" of Ploiesti Romania

Drying was made ty heating in oven at *120-130°C* for *4 hour/10Kg* powder.

After that was observed an adhesion between particles. For this reason mechanically we could brake these formed fragile adhesions. At dry grinding this phenomenon does not appear.

Metallic powders magnetic separation from abrasive powders was made with an electromagnetic plate.

Because metallic particles could retain fine abrasive particles, we have to pass the powder 3-4 times in front of the electromagnetic plate.

Analysing the stellite powders size distribution we observe that the separated magnetic powder has a majority distribution size smaller than *250 μm*. At rellite powders the dimension is greater because carbide grains are fixed in matrix and not dissolved like stellite.

Grain's size and distribution have a great importance at tube electrodes manufacturing. After chemical analyses, presented in table 1, we used to fill up *2.4 mm* and *4 mm* diameter electrodes with grain size smaller than *250 μm*.

Table 1. Chemical composition of magnetic separate stellit

Chemical element	Units [%]	Chemical element	Units [%]
C	2.17 ... 3	Mo	max 1.60
Cr	22 ... 12.5	Fe	max 1.03
Co	53 ... 57.2	abrasive disc powder	max 4.00
W	11.5 ... 12		

3. STRUCTURE AND WELD LAYER HARDNESS

Weld layers were made by oxyacetylenic method on carbon steel samples. Metallographic structure was made of fine carbides dispersed in matrix resulted by materials melting.

Structure homogeneity is improved at second and third stratum's layer. In fig. 1-3 we could observe the hardness variation as function of powder tips, number of stratums, electrode's wall tickness. Examining the curves we observe:

- near melting line hardness is the same, no mater the number of layer stratums;
- at weld layer with stellit tube electrodes, hardness is greater if we used great diameter electrodes;
- hardness is greater at the third stratum;
- hardness is greater at rellite electrodes;
- final tickness at wear exposed stratum has to be greater than *0.75 mm*.

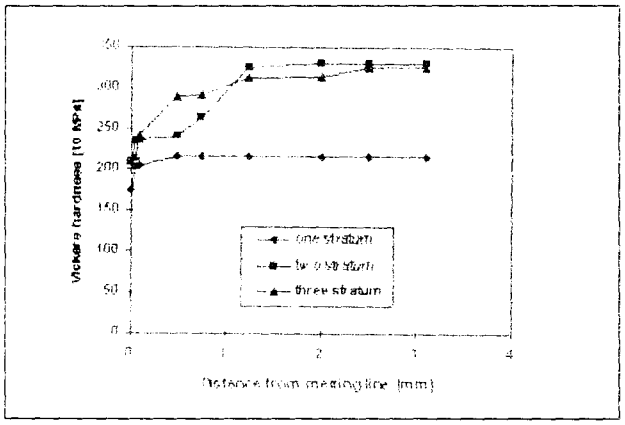

Fig. 1 Hardness variation for stellit electrode ϕ 2,4 mm

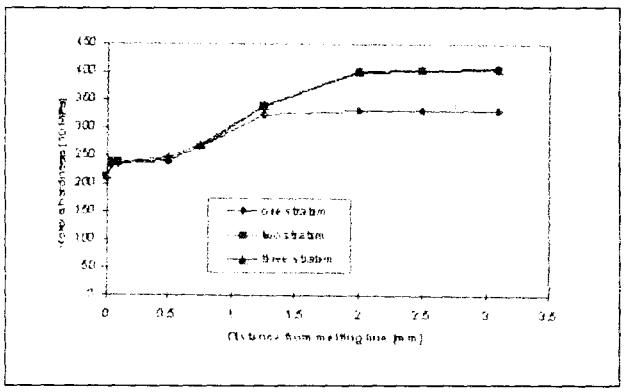

Fig. 2 Hardness variation for stellit electrode ϕ 4 mm

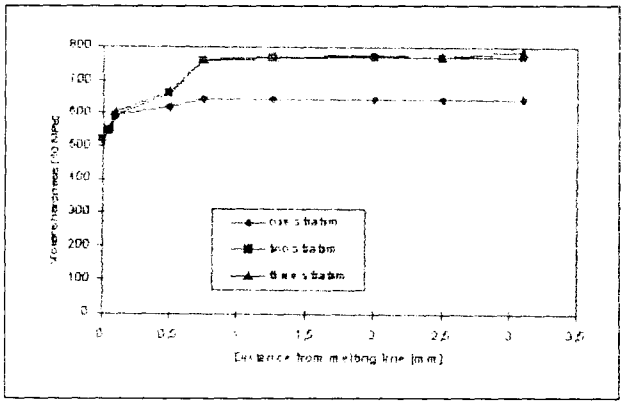

Fig. 3 Hardness variation for rellit electrode ϕ 4 mm

4. FRICTION COEFICIENT AND WEAR RATE

We determine friction coefficient fig. 4 and fig. 5 and wear rate fig. 6 on couple and machine Amsler. With 4 mm electrodes filled with rellit and with stellit samples were made covered with 1, 2, 3 stratums for Amsler shoe

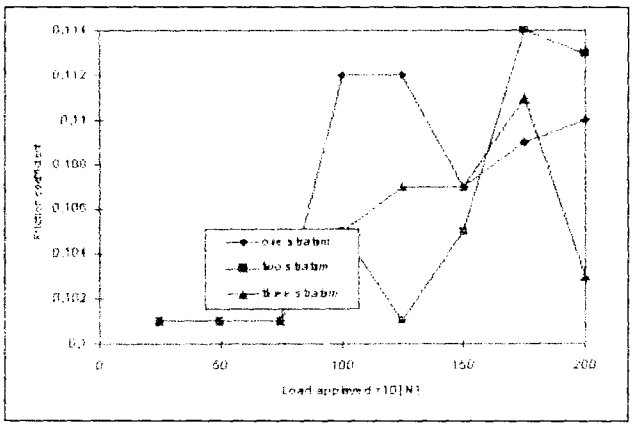

Fig. 4 Friction coefficient for rellit layers

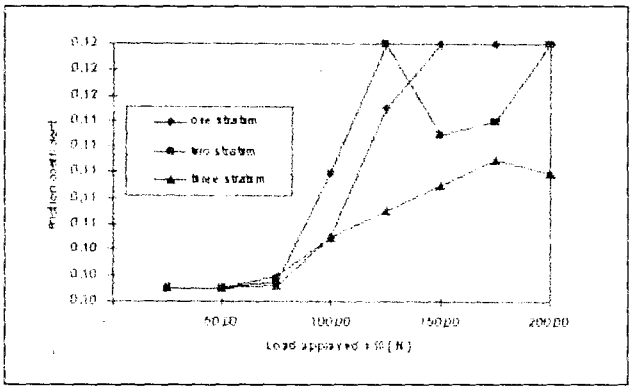

Fig. 5 Friction coefficient for stellit layer

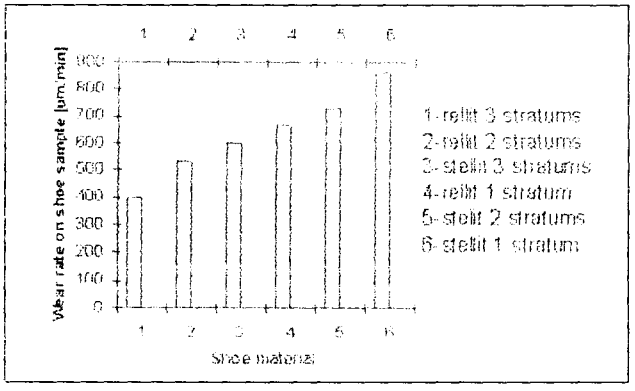

Fig. 6 Wear rate

sample. Roller material was a bearing steel with hardness 707HV, and *40 mm* diameter. Testing medium was oil for mechanical transmission.

5. CONCLUSIONS

We observe that smaller values for wear and friction coefficient were obtained for rellite three stratums weld layers. Also hardness values obtained recommend these recovered powders for medium hard wear weld coverings.

REFERENCES

[1.] *Tudor, I. and Rapeanu, R.*, **Fight against wear by weld covering with tube electodes**, ROTRIB, 96, 17, 59-64.